International Journal of Remote Sensing

ISSN: 0143-1161 (Print) 1366-5901 (Online) Journal homepage: http://www.tandfonline.com/loi/tres20

Airborne radiation mapping: overview and application of current and future aerial systems

D. Connor, P. G. Martin & T. B. Scott

To cite this article: D. Connor, P. G. Martin & T. B. Scott (2016) Airborne radiation mapping: overview and application of current and future aerial systems, International Journal of Remote Sensing, 37:24, 5953-5987, DOI: 10.1080/01431161.2016.1252474

To link to this article: http://dx.doi.org/10.1080/01431161.2016.1252474

Published online: 10 Nov 2016.

INTERNATIONAL JOURNAL OF REMOTE SENSING, 2016
VOL. 37, NO. 24, 5953–5987
http://dx.doi.org/10.1080/01431161.2016.1252474

Taylor & Francis
Taylor & Francis Group

Airborne radiation mapping: overview and application of current and future aerial systems

D. Connor[a], P. G. Martin [b] and T. B. Scott[b]

[a]School of Earth Sciences, University of Bristol, Bristol, UK; [b]Interface Analysis Centre, HH Wills Physics Laboratory, University of Bristol, Bristol, UK

ABSTRACT

Nuclear power and associated activities are never far from scrutiny, the apparent advantages of the technology are juxtaposed by the risk of incidents perceived as being catastrophic. If a major nuclear incident was to occur, an important aspect of the response management to any radionuclide release would be the need to rapidly establish the spatial distributions and quantities of these released radionuclides, their type in addition to their corresponding activity. The data received from surveys would directly inform evacuation plans, on-site incident management strategies as well as protecting both workforce and public from harm. The disaster at the Fukushima Daiichi Nuclear Power Plant in 2011 is perhaps the best example of the requirement for real time data collection to inform crucial decisions. Previous reviews of the event have observed that because the static on-site radiation detector network was destroyed by the 15 m high tsunami (following the magnitude 9.0 Great Tōhoku earthquake), it was not possible to immediately determine the radionuclide activity in the area and the danger presented to the responding workforce. Such preceding works have retrospectively highlighted the usefulness of unmanned aerial systems in providing real-time data within nuclear and non-nuclear settings. The establishment of an arbitrary 20 km exclusion zone surrounding the Fukushima Daiichi plant, with the displacement of over 150,000 people, has been viewed by many as an over-reaction – with many not having been required to be evacuated. This review examines and evaluates the previous as well as current work on aerial radiation monitoring and the future improvement that might be delivered by a combined three-dimensional (3D) radiation mapping platform. Combining detailed 3D topographical mapping with radiation surveying has powerful implications for the way that radiological contamination across a site might be measured and displayed in the future, both following radiological release events and in routine site monitoring.

ARTICLE HISTORY
Received 14 April 2016
Accepted 15 October 2016

- Comprehensive review of airborne radiation mapping.
- Exploration of potential future systems.
- Comparison of the multiple flight, mapping, and detection systems.
- Application of devices to a range of scenarios.

CONTACT P. G. Martin peter.martin@bristol.ac.uk Interface Analysis Centre, HH Wills Physics Laboratory, University of Bristol, Tyndall Avenue, Bristol BS8 1TL, UK

1. Introduction

Unmanned aerial vehicles (UAVs) for radiation mapping have been deployed on multiple occasions over the past decade (Kurvinen et al. 2005; Pöllänen et al. 2009). However, major technological acceleration within the field has been evident since the incident at the Fukushima Daiichi Nuclear Power Plant (FDNPP) in March 2011 (Boudergui et al. 2011; Cao et al. 2015; Furutani et al., n.d.; Han and Chen 2014; Han et al. 2013; MacFarlane et al. 2014; Martin et al. 2015; Sanada and Torii 2015; Towler, Krawiec, and Kochersberger 2012). Located off the eastern Japanese coast, the magnitude 9.0 earthquake and resulting 15 m high tsunami (Simons et al. 2011) destroyed the plants connection to the external power network and flooded the on-site back-up generators, leaving the reactor pressure vessels (RPVs) without adequate active cooling (Kurokawa, Ishibashi, and Oshima 2012; Povinec, Hirose, and Aoyama 2013). The ensuing rise in core temperatures initiated the highly exothermic reaction between the zirconium metal (Zircalloy) cladding material that surrounded each of the fuel rods and steam, which was released into the core following the opening of discharge valves used to alleviate the rising pressure within some of the RPVs (Kinoshita et al. 2011). This caused a series of large hydrogen explosions and the ejection of various radionuclides into the atmosphere from a number of reactors (Katata et al. 2012; Kinoshita et al. 2011; Lozano et al. 2011; Omoto 2013; Povinec, Hirose, and Aoyama 2013). Fallout spread primarily to the east over the neighbouring Pacific Ocean (80%) (Masson et al. 2011; Yoshida and Kanda 2012), with the remainder dispersing inland, principally to the northwest as a result of the prevailing wind direction (Yasunari et al. 2011); but in order to fully understand the extent of the contamination problem, detailed mapping of the affected areas was necessary.

The field of radiation monitoring can fall into two distinct categories: localization and mapping (Towler, Krawiec, and Kochersberger 2012). Localization (Jiang et al. 2015; MacFarlane et al. 2014; Pöllänen et al. 2009; Towler, Krawiec, and Kochersberger 2012) is the identification of an individual radioactive source, whereas mapping (Furutani et al., n.d.; Jiang et al. 2015; Martin et al. 2015; Sanada and Torii 2015) is rarely concerned with the location of a single emitter, and instead seeks to represent the distribution of radiation throughout a predefined area. Mapping is often used to quantify areas of risk; a tool that can be used to aid the decisions of governments and authorities, to protect a workforce or the public in the event of a disaster such as that which occurred at Fukushima Daiichi.

There are primarily three methods available with which to carry out the monitoring of radioactive material; static ground-based, mobile ground-based, and airborne surveys. When mapping high levels of radiation, such as those close to the site of the Fukushima release – the controlling factors over the choice of method relies on the protection of the workforce (due to safe standards governing radiation exposure, ≤20 mSv year^{-1} [IAEA 2003]) as well as the need for rapid data acquisition and presentation to assist in fine targeted mitigation methods, for example evacuation plans and the distribution of iodine tablets in order to combat potential ^{131}I exposure (Omoto 2013; World Health Organization 1999).

Static ground-based options typically involve a fixed device capable of measuring dose (radiation intensity) and preferentially also, spectroscopy to determine the

contributing radioisotopes present. Across a static network, accurate and detailed activity profiles of specific locations can be determined with interpolation of data between neighbouring points. The static capability however provides only a very limited oversight of the true spatial distribution of the activity within a given area. Accordingly data gaps or blind spots in the network could prove hazardous for workers (Sanderson et al. 1995). As a result, static monitoring is not suitable for upscaling to provide high-resolution results to large projects such as at Fukushima, but for more localized releases. *In situ* measurements are limited to the location of ground stations and, therefore, potentially present a biased distribution in sampling, with data confined near to these stations (Green 1987).

The other ground-based alternative are mobile surveys, conducted most frequently using either handheld or vehicle-mounted detectors. Handheld surveys involve the manual movement of a detection system around an area by a human, providing a good spatial resolution but requiring significant data collection time for larger areas. Moreover, this method is only applicable in accessible areas and where data collection is within the safe exposure limits of the operator, which make this method unsuitable for a first response survey due to the unknown intensity. In addition, the operator will attenuate a significant amount of the radiation that would otherwise reach the detector, reducing the measured intensities by 20–35% (Buchanan et al. 2016; Jones and Cunningham 1983). Whilst the housing around any detector will also shield radiation, the effect of this is less pronounced, systematically constant, and well constrained in comparison to human shielding – for which currently no comprehensive comparison currently exists for varying body types. Vehicle-mounted surveys have a much larger capability for coverage than handheld surveys, allowing for areas of 100 s of km to be mapped within a 24 h period (Mellander 1995). The absolute coverage is however limited to the extent of the road network, or the accessibility of the environment that the vehicle is travelling through. In order to maintain good spatial resolutions, the surveys must be undertaken at low speeds of around 13 m s^{-1} or less. More significantly though, the technique still involves the exposure of the driver to potentially harmful radiation in disaster scenarios, and as such does not present the ideal method to characterize unknown levels of contamination.

In comparison, airborne surveys are the most time effective way to quickly gather radiation data over large areas due to the high operational speed and lack of obstacles at the altitudes at which the surveys are conducted. Rates of coverage are up to 10^3 times that of car-based surveys, depending on the aircraft used (Schwarz, Rybach, and Klingele 1995). Additionally, those performing the survey are mostly removed from the risk of high-dose radiation exposure due to the operational altitude (≥120 m) (Schwarz et al. 1995), although flight trajectories which would pass through a radioactive fallout plume would still present a significant exposure to the operator and contamination risk to the aircraft. Despite being rapid, the initial expense of these systems is considerable (Guss 2011; MacFarlane et al. 2014; Martin et al. 2015) and aircraft are typically subject to strict regulations; including restricted flying zones, altitudes, and visibility restrictions (CAA 2015). The development of UAVs has removed much of the need for piloted surveys, having the ability to be remotely operated from a distance (up to 150 km) (Kurvinen et al. 2005) or to fly autonomously along a pre-defined way-pointed flight path. Such an approach removes the possibility of endangering first responders and

survey workers within post-disaster environments. Moreover, UAV technology is considerably less expensive than the alternative human piloted option (MacFarlane et al. 2014). In most countries, the restrictions upon UAVs are typically less stringent than for higher altitude and heavier airborne methods. In the UK, for example, aircraft under 7 kg (CAA 2015) are limited to a maximum flight altitude of 122 m and are treated differently on the basis that they represent less danger of structural damage to buildings should an accidental impact occur. In the case of such low altitude radiation mapping, the nature of the UAV systems allow for the collection of data quickly and independently of terrain with limited radiation shielding effects when compared to a human operator.

2. Aircraft system

Research into radiation surveying or mapping using UAVs has occurred for a range of scenarios, these include; ground-level radiation following post-disaster environments (Furutani et al., n.d.; Jiang et al. 2015; Sanada and Torii 2015; Towler, Krawiec, and Kochersberger 2012), airborne plumes (Kurvinen et al. 2005), low-level radiation anomalies (MacFarlane et al. 2014; Martin et al. 2015), indoor applications (Boudergui et al. 2011) and theoretical tests (Boudergui et al. 2011; Han and Chen 2014; Han et al. 2013; Jiang et al. 2015; MacFarlane et al. 2014; Pöllänen et al. 2009; Towler, Krawiec, and Kochersberger 2012)

Previous studies have explored a variety of UAV designs (Table 1). These range from fixed-wing (Kurvinen et al. 2005; Pöllänen et al. 2009) to single rotor helicopter-style aircraft (Furutani et al., n.d.; Sanada and Torii 2015; Towler, Krawiec, and Kochersberger 2012) and multi-rotor systems (Boudergui et al. 2011; Han and Chen 2014; Han et al. 2013; MacFarlane et al. 2014; Martin et al. 2015). In comparing these works, a number of similarities and differences can be highlighted in the attributes of each of the systems. Studies involving fixed-wing systems (Kurvinen et al. 2005; Pöllänen et al. 2009) demonstrate a high top speed (240 and 120 km hour^{-1}, respectively), alongside a high cruising velocity (90 and 60 km hour^{-1}, respectively). This enables the systems to have excellent ground coverage during a single flight. As noted in Sanderson et al. (1995) and MacFarlane et al. (2014), this capability comes at an inherent loss of spatial resolution. In Kurvinen et al. (2005) the detectors were set to sample data integrated over 10 s collection interval. Even if the UAV in the study was travelling at the lowest speed achievable, this would equate to a highest potential spatial resolution (not including the important effect of altitude) of 250 m per measurement. An increase in the rate of data acquisition would improve the spatial resolution – for example, Pöllänen et al. (2009) had a similarly fast vehicle, but with a data acquisition rate of 1 measurement per second, yielding an improved spatial resolution equating to approximately 17 m ground area per measurement. In contrast, helicopter-style and multi-rotor systems are able to hover in a stationary position, and hence travel at much lower speeds and altitudes, producing data at significantly higher spatial resolutions. In some cases, operational velocities of between 1.5 and 8.0 m s^{-1} have been achieved (MacFarlane et al. 2014; Martin et al. 2015; Sanada and Torii 2015). This is a direct result of the increased stability that is inherent within their design, with these systems even being capable of being flown without a professional pilot, in weather conditions more adverse than for larger fixed-wing platforms (Martin et al. 2015). Whilst not mentioned within the reviewed

Table 1. Summary of existing aerial vehicle systems and associated detection options.

	Kurvinen et al. (2005)	Pöllänen et al. (2009)	Sanada and Torii (2015)	Towler, Krawiec, and Kochersberger (2012)	MacFarlane et al. (2014)	Martin et al. (2015, 2016)	Han et al. (2013, 2014)	Furutani et al. (n.d.)	Boudergui et al. (2011)
Model	Ranger ADS-95	PATRIA MASS mini UAV	Yamaha RMAX G1	Scout B1-100	Hexa-XL Mikrokopter	Custom built UAV	Foam RC aircraft	RobinPARS	CEA X4-Flyer
Length (m)/ wingspan (m)	4.6/5.71	1.05/1.50	3.63/1.08	3.30/1.30	1.00	1.30	1.22	1.83/1.00	c. 0.50
Weight (kg)	Unspecified	3.00	94.00	50.00	2.20	6.80	1.50	11.80	0.90
Payload (kg)	45.00	0.50	10.00	18.00	1.50	1.50	0.70	5.00	0.20
Flight speed (km hour^{-1})	90–220	60–120	Up to 72	Unspecified	Up to 75	Up to 70	54	Unspecified	Unspecified
Endurance (minutes)	240	60–75	90	90	12	30	70	60	15
Power source	Petrol	Battery	Petrol	Petrol	Battery	Battery	Battery	Unspecified	Battery
Operational altitude (m)	Normal flight altitudes	50	80	60	3–15	3–15	50–200	250	3–15
Operational range (km)	100	Unspecified	Up to 0.4[a]	Unspecified	Within sight[b]	Within sight[b]	1.6	>20	0.1[c]–1.5[d]

[a]Visible range.
[b]Range limited to line-of-sight by regulations imposed by the UK CAA.
[c]Indoors.
[d]Outdoors open space.

literature, some of the discussed issues relating to fixed wing aircraft could be addressed with the implementation of the new Vertical Take-off and Landing (VTOL) systems. Such systems have the enhanced ability to take off in small/restricted areas and hover statically over areas of interest.

Whilst operational velocity must be considered important, the greatest factor impacting on the spatial resolution of the final map is the altitude at which the survey is conducted (Martin et al. 2015; Sanderson et al. 1995; Schwarz, Rybach, and Klingele 1995). For an idealized radioactive point source, the intensity (I) of the radiation at any altitude/distance (z) can be modelled as following an inverse square relationship:

$$I \propto \frac{1}{z^2}. \tag{1}$$

This effect, shown diagrammatically in Figure 1, can be seen in the results from Pöllänen et al. (2009) and Sanada and Torii (2015), with altitude impacting directly on the resolution achieved (Figure 2). When mapping non-point source emitters, the radiation excess emitted from the ground can be determined through calibration with background (best obtained above water where only cosmic background is encountered) and mathematical modelling (Furutani et al., n.d.).

The operational altitude of the UAV can be crudely related back to both its size and manoeuvrability. The large fixed-wing UAV utilized in Kurvinen et al. (2005) operates at high altitudes (maximum of 4500 m) due to its considerable size (4.6 × 5.71 m) and high operational velocity (90 km hour^{-1}). This vehicle would not be suitable for low altitude

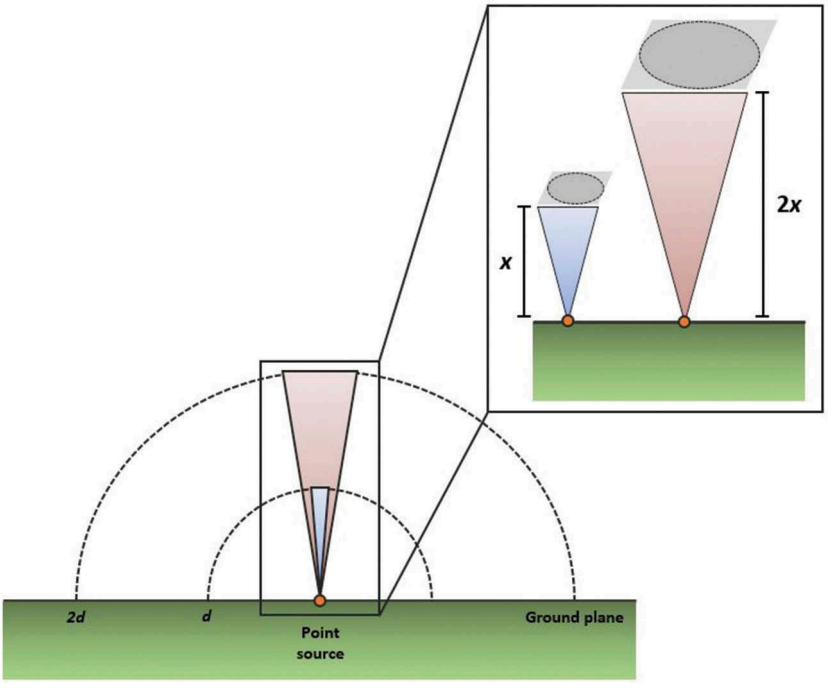

Figure 1. Schematic illustrating the inverse square law from a point source with the impact of distance on achievable resolution.

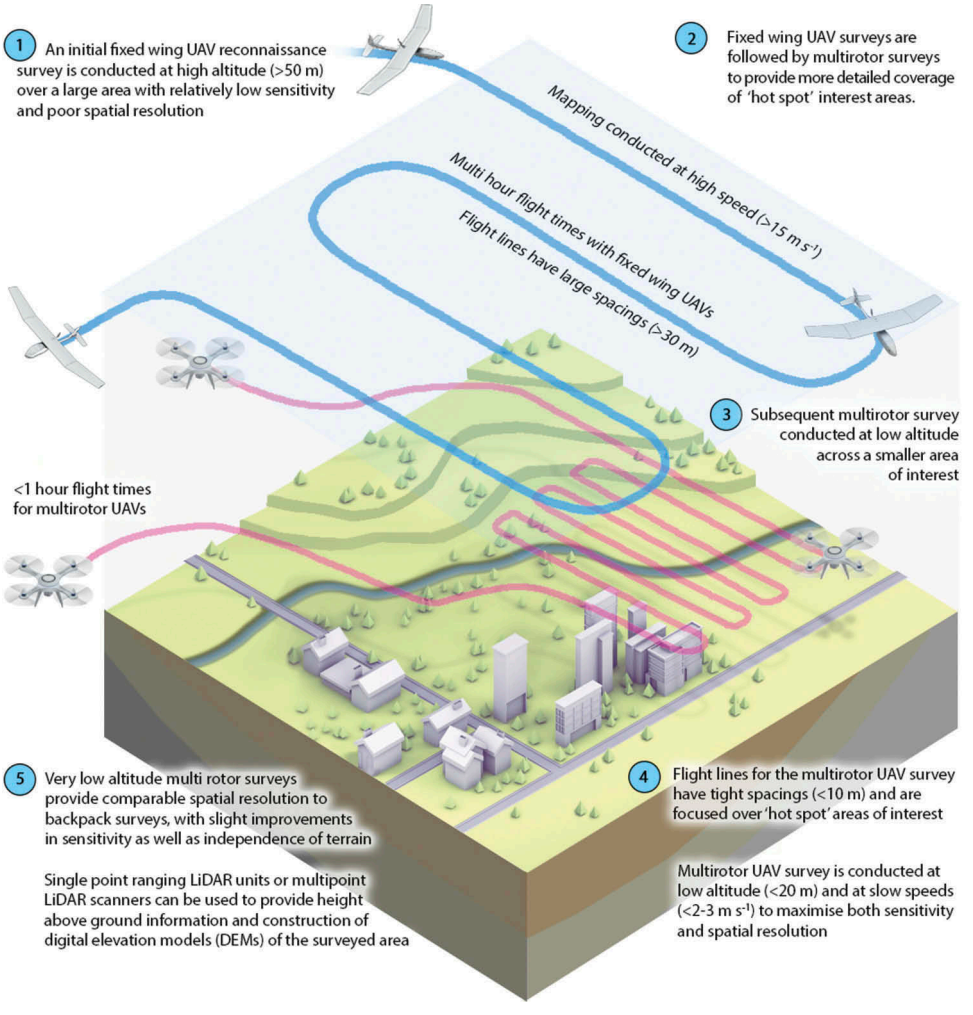

Figure 2. Differing survey resolution achievable via contrasting survey methods, including high-altitude fixed-wing and multi-rotor UAV.

surveys (<122 m) due to the topographical and anthropogenic obstacles that exist at these heights. Helicopter-style UAVs (Furutani et al., n.d.; Jiang et al. 2015; Sanada and Torii 2015; Towler, Krawiec, and Kochersberger 2012) have been shown to successfully operate at reduced altitudes of around 60–80 m, still well above that used by the multi-rotor systems (Boudergui et al. 2011; Han and Chen 2014; Han et al. 2013; MacFarlane et al. 2014; Martin et al. 2015). Pöllänen et al. (2009) demonstrated that low altitude surveying (50 m) can be achieved by small fixed-wing UAVs, but this study focused on a scenario in which radioactive point sources were located within an airfield. Whilst this is a necessary simplification to test a technique, it remains to be seen if it can be applied successfully to non-fictitious situations where obstacles may exist at the operating altitude. In addition, the speed at which the UAV must operate also reduces the resolution of the radiation map produced. With no technological increase in the logging/data collection rate of the detection system, producing high resolution maps

requires an increased 'dwell' time to complete an adequate survey for a given area. Whilst Sanada and Torii (2015) showed that the lower altitude and slower speed of the UAV compared to the full size fixed-wing aircraft produced a higher resolution map, it took a total of 52 days to complete the aerial survey. This is a product of the typical flight times that can be achieved by each data collection run. For example, the UAV system presented in Martin et al. (2015) was powered by batteries that allow for between 30 and 40 min of flight time per charge. Other battery run systems (Boudergui et al. 2011; Han and Chen 2014; Han et al. 2013; MacFarlane et al. 2014) display similarly small individual flight time (12–30 min). Conversely, systems that run on petroleum fuels (Kurvinen et al. 2005; Sanada and Torii 2015; Towler, Krawiec, and Kochersberger 2012) tend to have longer individual flight times (90–240 min). Whilst this longer flight endurance allows for greater amounts of data to be collected, the weight of the system is significantly increased relative to those operating on battery power, with stricter regulations placed upon systems heavier than 7 kg (CAA 2015). Whilst the collective survey time of light weight battery powered UAVs can be streamlined through using multiple batteries on rotation (Martin et al. 2015), the approach is still inherently limited by the rate of advancement in battery technology.

In planning an airborne radiometric survey, the primary focus of the study needs to be established. Defining factors such as the spatial extent of the study area, the required spatial resolution and the maximum survey time permissible are to be constrained in order to implement the most suitable platform for the survey. For example, large fixed-wing aircraft systems remain best suited to first response situations following large-scale releases of radioactive material (e.g. Fukushima or Chernobyl disasters). In these situations, rapidly establishing radiation dose rates to aid evacuation and disaster management plans is the primary focus. These systems provide the most temporally efficient method of defining radiation intensity over regional and/or even national scales, a feat which cannot be matched by current UAV technologies within the same timescale.

On the other hand, large fixed-wing aircraft are not suitable for producing more detailed high-spatial resolution radiation maps, which require a platform capable of operating at lower altitudes and slower speeds. Higher resolution surveys are required in scenarios where more localized variations in radiation intensity are important (i.e. in localizing a specific radioactive point source, radioactive mineral exploration and monitoring work in nuclear facilities or low-level radiation anomalies). In such scenarios, helicopter-style and multi-rotor configurations are much more suitable, providing the ability to cover areas with tightly spaced flight lines, flying at low speed and altitude, and flying relatively close to structures on the ground without significant risk of collision. Equally, in such scenarios the aircraft do not need to carry such large radiation detection systems due to their relatively close proximity to ground-based radiation source.

By integrating both fixed-wing/helicopter style and multi-rotor systems, there is the potential for excellent temporal coverage without the need to compromise on spatial resolution. For example, using the increased speed and range of the fixed-wing/helicopter installations, a large study area can be sampled rapidly (Figure 2(*a*)). Any identified hotspots/areas of interest can subsequently be investigated in greater detail using a multi-rotor system at a reduced speed and altitude to increase the spatial resolution (Figures 2(*b*) and (*c*)).

3. Detection systems

3.1. *Basic detector principles*

Gamma-rays interact with matter through three principle methods: The photoelectric effect; Compton scattering and pair production (Grodstein 1957a; Hubbell 1969; Knoll 2010; Leclair 2010). The efficiency of a gamma-ray detector is a function of its sensitivity to any incident radiation (counting efficiency) and its active volume. Unlike detectors for alpha and beta radiation (charged particles with much easier detection), an incident gamma ray photon must have a significant interaction with matter within the active volume of the detector to produce a discernible signal (Knoll 2010). With any gamma-ray detector, some of the incident radiation will simply not interact with the detecting matter because not all incident photons will be intercepted, and their energy absorbed by the detector medium. The ratio between the amount of radiation incident on a detector and the measured radiation is known as the 'intrinsic counting efficiency' (Knoll 2010); simplistically a function of electron density of the interacting detector material (the probability of a photon interaction increases with increasing density).

There are a number of different variations within gamma ray detector technology. These variations differ from each other in terms of the active material used, count collection methods and the mode of the detector (Knoll 2010). However, by analysing the basic operation of these systems, a simplistic model of gamma ray detection systems can be identified. Upon the interaction of a single gamma ray with the active detection material (e.g. scintillating or semi-conductor crystal), a resultant release of electrical charge occurs within the detection system (or is indirectly formed through the use of a photomultiplier tube, as is the case with scintillator detectors). This electrical charge is then collected through manipulation of the voltage imposed across the active detector material, causing the positive and negative charges created by the interaction to flow to opposite electrodes (Knoll 2010). The time taken for the detector to fully accumulate the resultant charge is different across the range of detector types; a combination of the mobility of the charge carriers within the active volume and the average distance that needs to be travelled through the active volume to reach the corresponding electrode (Knoll 2010). In general, instruments that employ solid detector materials (scintillator and semi-conductor detectors) with rapid counting times may be considered as better suited to mobile radiation surveying because the effect of spatial averaging is reduced.

3.2. *Detector systems in UAV radiometric surveys*

The payload employed for mapping typically consists of a GPS, radiation detector(s) coupled to a data storage and processing unit to locally store data on the device before (optionally) being transmitted to a base station. In some cases, the objectives of the investigation called for extra equipment within the payload, for example air samplers (Kurvinen et al. 2005; Pöllänen et al. 2009) or single-point laser range-finders (MacFarlane et al. 2014; Martin et al. 2015). An ideal detector configuration would employ a very high density material for a high counting rate and a large volume. Whilst such a detector would not be suitable for deployment on a UAV due to its weight, a swarm of UAVs could be implemented to establish static monitoring points

within a target zone. Using a number of these systems equipped with the traditional smaller volume detectors in a single target survey is a potential solution for the inherent loss of 'stopping power' experienced by these detectors. Moreover, by hovering these at defined points/intervals around a target area, a monitoring ring of detectors is established, which can be used to effectively localize radioactive sources, or determine a local radiation intensity state (see Section 4 for further details on this). Detectors used in the studies detailed herein vary between a number of different types, including; scintillator detectors (Furutani et al., n.d.; Kurvinen et al. 2005; Pöllänen et al. 2009; Sanada and Torii 2015; Towler, Krawiec, and Kochersberger 2012), Geiger–Muller (GM) tubes (Kurvinen et al. 2005), and semiconductor detectors (Kurvinen et al. 2005; MacFarlane et al. 2014; Martin et al. 2015).

The use of GM tubes for radiation detection systems was employed in early UAV studies (Kurvinen et al. 2005). These detectors are simple inert gas filled units containing opposing positive and negative electrodes. Incoming radiation causes ionization of the gas, with the resultant positive ions and negative electrons attracted towards the relevant electrode, generating an electronic pulse (count). Whilst the detectors are lightweight and high volume, they have an inherently very low sensitivity compared to the other detector types used (Knoll 2010), and since Kurvinen et al. (2005) they have not been employed for UAV radiation monitoring.

There are numerous scintillator materials available for use as radiation detection materials, however, for use within an UAV format there are three common materials used; $LaBr_3$[Ce] (Sanada and Torii 2015), NaI (Furutani et al., n.d.; Kurvinen et al. 2005; Towler, Krawiec, and Kochersberger 2012), and CsI (Han and Chen 2014; Han et al. 2013; Pöllänen et al. 2009). CsI and NaI scintillator detectors have similar characteristics; they are both alkali halide compounds that display good scintillation properties when the pure crystal is doped with certain impurities. Their differences however, arise from the variation in the physical properties of the materials. NaI is a lower cost material than CsI and is in greater abundance, but is hygroscopic and, therefore, deteriorates through prolonged water absorption into its structure (Knoll 2010). As a result the material is required to be housed within an airtight chamber during use, which adds weight to the system. CsI is less hygroscopic and much less brittle as a material, capable of withstanding more vibration and shock (Knoll 2010), making it is more durable and more suitable for use as an airborne detector. Both materials can be activated with additional components (thallium for NaI and sodium/thallium for CsI) to improve their scintillating properties and resolution for identifying particular radionuclides within the output spectra (Knoll 2010). When activated, the CsI detectors have a larger gamma-ray absorption coefficient per unit size than NaI detectors, making them more applicable for small sized detectors (Knoll 2010). However, NaI produces a greater photon brightness, meaning it produces the most easily discernible electric signal following the interaction of radiation within the active volume of the detector (Knoll 2010). Activated CsI detectors were used within Han and Chen (2014) and Han et al. (2013) but it is not specified within any of the studies using NaI detectors whether they are activated, hence these studies will have less well resolved spectra than those that use activated scintillators (CsI[Na] or $LaBr_3$[Ce]).

A cerium-activated lanthanum bromide ($LaBr_3$[Ce]) detector (Sanada and Torii 2015) provides a better energy resolution than both NaI and CsI (Knoll 2010).

However, the material is also hygroscopic, requiring an airtight chamber to avoid material degradation (Shah et al. 2003), with the further addition of weight to the system. The $LaBr_3$[Ce] detector in Sanada and Torii (2015) displayed a full width at half maximum (FWHM) value of 2.8% at 662 keV, whereas standard values for activated NaI and CsI are 7.5–8.5% (Canberra 2014) and <7.2% (Kromek Group PLC 2015) at 662 keV, respectively. A spectra from this type of detector though does not show as good pulse shape discrimination as NaI or CsI; making it difficult to identify the contributing species (Knoll 2010). This poor peak shaping, however, does not represent a problem when mapping in post-disaster zones as for Sanada and Torii (2015), where radioactivity is almost entirely associated with the fission products of ^{131}I, ^{134}Cs, and ^{137}Cs (Bolsunovsky and Dementyev 2011; Buesseler, Aoyama, and Fukasawa 2011). However, for mapping low-level radiation anomalies, a $LaBr_3$[Ce] detector would not represent an appropriate detector choice.

An alternative to scintillator type detectors are cadmium zinc telluride (CZT) detectors. These are a variant of semi-conductor radiation detectors, which use the ionization of the semi-conductor by the incident gamma radiation and subsequent movement of the produced electron hole pairs to opposing electrodes in order to produce electrical pulses (similar to gas ionization methods [Luke 1995]). Such pulses are detected, and processed to produce a gamma spectrum. The material has a very high mass number (*A*), creating a very good counting efficiency – as the likelihood of interaction between the material with incident radiation is increased relative to other materials (e.g. air, water, and lead illustrated for comparison (Figure 3)) and NaI/CsI scintillators (Luke

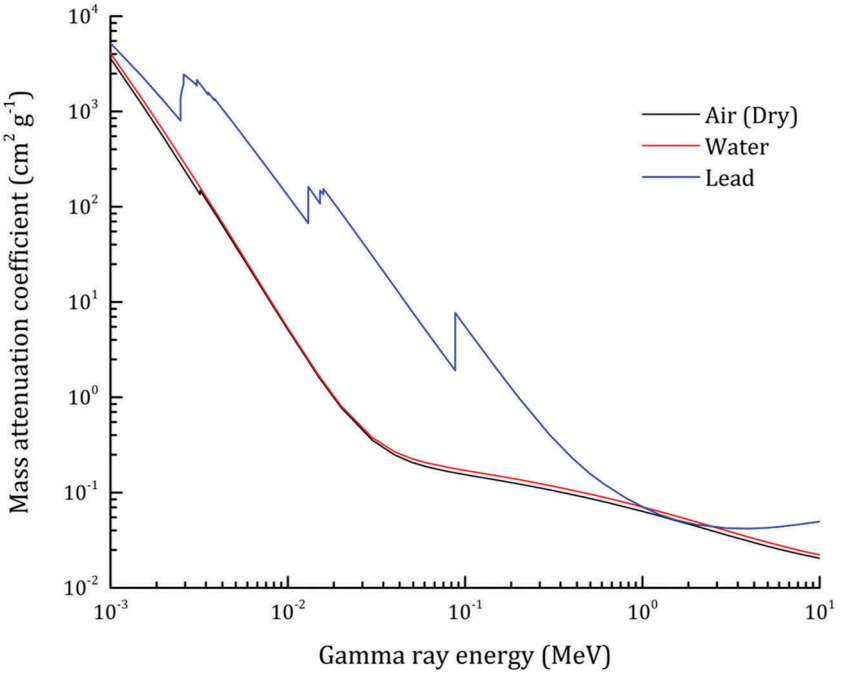

Figure 3. Differences in mass attenuation coefficients for three selected materials; air (dry), water, and lead across the full gamma-energy range (from NIST).

Table 2. Summary of detector types used along with their associated advantages, disadvantages, and typical energy resolution.

Geometry type	Advantages	Disadvantages	Typical energy resolution (FWHM) (%)
Planar electrode	Simple structure	Severe hole trapping problems	–
Frisch strip and trapezoid prism electrode	Simple structure	Existing leakage currents between the grid and anode	2.68 [at 662 keV]
Insulated Frisch ring electrode	Eliminating leakage currents between the grid and anode	More complicated design and fabrication technique	1.70 [at 662 keV]
Pixelate electrode	Higher charge collection efficiency; suitable for medical imaging	Charge sharing problems	<3 [at 140 keV]
Coplanar grid electrode	Overcoming hole trapping more efficiently	Needing more output readout electronics; more electrical noise	1.3% [at 662 keV]
Hemispherical electrode	Uniform charge collection	Complicated geometry design	<1.9 [at 662 keV]
Orthogonal coplanar strip electrode	Less complexity for the device electronics	Leakage current in anode	1.0 [at 662 keV]
Charge-sharing strip electrode	Simplified electronics and more efficient non-collecting signal	More electrical noise	<6 [at 122 keV]
Drift strip electrode	Sensitivity to hole trapping is reduced due to the electrostatic shield to the readout anode	More electrical noise	0.8 [at 356 keV]

1995; Sellin 2003; Wilson et al. 2011; Zhang et al. 2013). A further advantage of CZT is that the material can be manufactured into different shapes, for example co-planar grids and small pixel detectors to optimize for differing applications. This therefore improves detection characteristics (Table 2) (Luke et al. 2001; Luke 1995; Wilson et al. 2011), however the co-planar grid variation produces the best energy resolution of any of the detectors previously discussed (<2.5% at 662 keV) (Chen et al. 2008; Martin et al. 2015; Sellin 2003; Zhang et al. 2013), allowing for the production of the most resolved energy spectrum and hence the most confident identification of individual radionuclides (although Table 2 indicates that this could still be improved upon). Despite this high resolution, problems with the uniformity of the crystal structure, such as random grain boundaries, have limited its effectiveness by causing charge trapping – reducing the counting efficiency in certain applications and limiting the volume of the detectors to small sizes, i.e. 1 cm^3 (Luke et al. 2001; Zhang et al. 2013). However, recent work into new methods of crystal manufacture through the travelling heater method (THM) process (Chen et al. 2008; Wilson et al. 2011) has yielded promising results to improve crystal uniformity and, therefore, allow for the volume of detectors to increase. Conceptually ultra-dense semi-conductor materials such as diamond and uranium dioxide (UO_2) could be considered and adapted for UAV applications, and are currently being developed. However, they have yet to achieve any commercial maturity which is unlikely for several years to come.

The active material within a detector is not the only consideration when designing a detector system; the directionality and shape of the material are also important. Detector directionality describes the changing response of the detector to incoming radiation at different interception angles. Incident photon trajectories not along the

symmetry axis of the active material can reduce measured intensities by between 20% and 30%, most notably in crystalline materials (Knoll 2010). The principle can however be reversed to be advantageous. By measuring the count-rate variation over individual sections of the active material volume, an angle of incidence can hence be calculated (Uher et al. 2007). This angle could be used to infer an azimuth from the detector in the general direction of the source, allowing for localization.

Gamma imaging (Jiang et al. 2015) has also been considered as a further technique for the localization of radioactive sources. Gamma cameras provide two-dimensional (2D) images from emitted gamma radiation on a target, using a single large volume detector (classically NaI), arranged to form a flat face, with an array of photomultiplier tubes on one side and a lead/tungsten collimator with an array of parallel pinholes on the other. The lead collimator restricts the gamma radiation entering the detector so the image can be directly interpreted as a reflection of the radioactive source (Knoll 2010). Gamma cameras could be adapted to quickly localize hotspots within an area, provided that radiation intensity was high enough to produce discernible signals over the exposure period of the camera. Theoretically, the data received to generate the image could also be used to fingerprint the radionuclide responsible through acquisition of a gamma spectrum. Although the weight of such a system, due to the lead collimators required for its operation, would greatly limit its deployability on an aerial system.

Similarly to the criteria for deciding upon a suitable airborne platform, the most suitable choice of detector type depends on the nature of the environment and likely radiation characteristics within the study area. Certainly, the weight in addition to the volume of the detection system will have a significant influence on the type of aircraft selected for any mapping application. Increasing payload weight will always lead to a decreasing flight times for surveys.

4. Algorithms for radiometric surveys

4.1. *Algorithms for radiation mapping*

As previously defined, radiation mapping describes the process of recording the level of radiation intensity at numerous points throughout an area and displaying the data in terms of position and a measure of intensity (gross count, activity, or dose rate are common units) in a graphical form. Across the reviewed literature, there is a general framework that can be identified in order to implement a radiation mapping survey. Simplified into three steps, this algorithm consists of: (1) establishing a calibration model, (2) data acquisition/normalization, and (3) presentation.

A basic calibration model for airborne radiation mapping requires an estimate of the variation in measured intensity with increasing distance. For simplicity, aerial radiation mapping is often conducted at a fixed altitude above ground level (AGL) (for example 80 m AGL [Sanada and Torii 2015]) and so variations in measured count rate (assuming the source is present at ground level) need to be appropriately modelled to a distance in excess of this altitude. Whilst emitted gamma radiation can be appropriately modelled by an inverse square count rate reduction over small source–receiver distances, this is not the case over the distances experienced within most applications of airborne radiation mapping (Knoll 2010) (with the exception of extremely low altitude surveys

[MacFarlane et al. 2014; Martin et al. 2015]). At larger distances, a reduction in count rate from attenuation through interaction with the constituents of air or other obstacles (explained in Section 5) becomes an important factor to consider. Hence, a more robust model is required.

The most commonly used method to acquire the calibration model is through a 'hover survey' (Furutani et al., n.d.; Sanada and Torii 2015; Schwarz et al. 1995). A 'hover survey' involves using a helicopter or other aerial platform to gather a profile of measured intensity over a fixed point on the earth by measuring intensity at a number of different altitudes. In general practice, the final maps produced from airborne radiation mapping projects are usually normalized to show intensity at one meter above the ground surface (Furutani et al., n.d.; Martin et al. 2015; Sanada and Torii 2015; Schwarz et al. 1995), which requires the calculation of the calibration curve. By measuring at defined intervals from a fixed point on the surface, a vertical profile of count rate reduction can be interpolated and used to extrapolate count rates at the surface, from the measured count rate at the operational altitude. Furthermore, as surveys are usually undertaken at a constant altitude from the starting point, some correction in terms of the variability in surface topography is required to accurately extrapolate measured intensity to surface intensity (Furutani et al., n.d.; Martin et al. 2015; Sanada and Torii 2015). To apply this correction, some studies have used digital elevation models (DEMs) to gather surface topography information and used the elevation data from these to apply an altitude correction (Furutani et al., n.d.; Sanada and Torii 2015). More recently, a lidar module (single-point range-finder variation) was used to determine actual altitude AGL to a millimetre scale accuracy (Martin et al. 2015). This method provides specific, high accuracy altitude data at every data point sampled by the detector within the mapping flight, which dramatically reduces the error within the calculated surface intensity compared to the use of DEMs.

The calculated calibration curve is also useful in other ways. As the output from the radiation detectors used within these mapping applications is often quantified in terms of counts per second (CPS). Simply, this corresponds to the cumulative number of detectable interactions occurring within the active volume of the detector over a time period of one second. From this information, hotspots and regions of low intensity can be identified. However, in a practical application of identifying risk, this means little to a responding taskforce. Instead of CPS, many maps are presented in terms of the dose rate (Furutani et al., n.d.; Sanada and Torii 2015), as this directly relates the radiation intensity into a value received by the body over a given time, which can be measured and the effective steps taken to make sure that any exposure is controlled or avoided. Converting the CPS into a dose rate value requires knowledge on the source, its activity, and the variability of these with distance; these form another part of the reason why a calibration model is required.

As the main focus of radiation maps can vary from one map to the next, further calibration parameters may need to be calculated or estimated in order to calculate the target parameter of a particular study. An example of this can be found within Sanada and Torii (2015). In part, this study looked to estimate the contribution of radiocaesium isotopes (released into the environment following the Fukushima incident) from the total radiation intensity experienced at the test locations. In order to do this, an estimate of the background intensity (contribution of cosmic radiation, inherent radiation

associated with the $LaBr_3$ detector, and any contamination present on the hosting UAV) was required to subtract from the total intensity recorded by the detector. This value was estimated through implementation of a fixed altitude hover survey over deep water, as the water body acts as an attenuator for any radiation emitted from the ground surface, leaving only that which is associated with the background intensity.

Once the calibration model and parameters have been calculated, the data collection for the map can be undertaken. In order to maintain the best compromise between ground coverage and temporal efficiency, the flight path of an airborne radiation mapping system requires the correct flight line spacings. Calculating the most appropriate spacings requires the operator to work out the effective ground sampling area of the detector; a function of the flight altitude and aperture of the detector (Knoll 2010, 118). The optimum line spacing incorporates overlapping regions between the areas sampled within each flight line with the previous/next flight line. This occurs because the counts received by the detector at the edges of the sampled ground will be reduced relative to the same source strength placed immediately below the detector (as incident radiation incoming to the detector at larger angles produces a reduced interaction) (118). Following the completion of the data collection, the values are normalized (usually to a height of one meter AGL) using the calibration model and converted into the relevant units. For converting CPS into dose rates, this can be achieved through using a radioactive dosimeter to measure the dose rate across the target area (if possible) (Sanada and Torii 2015) or using laboratory experiments (with the dosimeter) to determine the CPS/dose rate conversion factor. With this factor established, converting the units within the map is a trivial process.

Presenting the collected data as part of a map generally consists overlaying a colour scaled intensity representation onto a two dimensional map/spatial representation of the mapped area (Furutani et al., n.d.; MacFarlane et al. 2014; Martin et al. 2015; Sanada and Torii 2015; Schwarz, Rybach, and Klingele 1995). There are a number of ways in which this can be done, however most commonly used are geographic information system (GIS) products, as these offer a large degree of versatility and control over all the aspects of the final map. Whilst there has been much advancement in terms of detector technology and aerial platforms within in the past, little consideration seems to have been paid in advancing the way that the mapping data is presented. Even though there is a clear improvement between the map visualization in Martin et al. (2015) and Schwarz et al. (1995), the basic principle remains unchanged.

4.2. *Algorithms for radioactive source localization*

The process of locating a radioactive source relies upon determining its position from measurements of radiation intensity at different points in space within a given area. Unlike radiation mapping, it uses the information recorded by the detector to extrapolate backwards to a specific ground location for a given point source. Implementing this requires knowledge of the relationship that exists between the intensity of the source and the distance between the source and detecting instrument (in three dimensions). This relationship follows an inverse square approximation (discussed previously), whereby the measured intensity at the detector interaction volume (in cm^3) (λ_k) is a function of the intensity of the source (I), the position of the detector (x_k, y_k, z_k), the

position of the source (x_0, y_0, z_0) and a defined measured background intensity for the study area (λ_b) (Equation (2)) (Towler, Krawiec, and Kochersberger 2012):

$$\lambda_k(x) = \frac{I}{(x_k - x_0)^2 + (y_k - y_0)^2 + (z_k - z_0)^2} + \lambda_b. \quad (2)$$

Inverse square law from Towler, Krawiec, and Kochersberger (2012) (2)

A number of statistical algorithms have been highlighted within the published literature as effective in providing estimates of source locations based on radiation data acquired from a specified area. Whilst each of the individual algorithms differ in terms of the specific statistical models used or the assumptions made with respect to the initial model conditions (i.e. assumption of a known source radionuclide or intensity), each is based around the Poisson distribution of radioactive decay and emission (Brennan, Mielke, and Torney 2005; Knoll 2010; Muske and Howse 2001; Towler, Krawiec, and Kochersberger 2012). At high radiation intensities, the Poisson distribution equates well to a Gaussian distribution (Brennan, Mielke, and Torney 2005; Towler, Krawiec, and Kochersberger 2012).

The reviewed algorithms include recursive non-linear least squares optimization algorithms (Howse, Ticknor, and Muske 2001), several variations on recursive Bayesian estimation (RBE) algorithms (Brennan, Mielke, and Torney 2005; Brewer 2009; Morelande, Ristic, and Gunatilaka 2007; Muske and Howse 2001; Towler, Krawiec, and Kochersberger 2012), maximum likelihood estimator (MLE) algorithms (Gunatilaka, Ristic, and Gailis 2007; Morelande, Ristic, and Gunatilaka 2007) and mapping-based localization techniques (Towler, Krawiec, and Kochersberger 2012)

4.2.1. *Recursive non-linear least squares optimization algorithms*

Work conducted within Howse, Ticknor, and Muske (2001, 1727–1737) utilized a non-linear least squares optimization algorithm to track a single moving source within a room in real time. To begin, four individual gamma detectors were located in each corner of the room, and used to estimate the potential positions a ^{137}Cs source of known intensity using level curves derived from the measured counts at each detector; with the intersection point of these four curves marking the most probable location. Due to the variability in the measured count rate, these curves manifest as shells rather than lines, creating an intersection zone. A single point estimate was produced by running the non-linear least squares optimization to minimize the residuals between the estimated locations from each of the four detectors. With this initial state confirmed (including the background radiation for the room), a tracking algorithm is then used to iteratively predict the movement of this source throughout the room by detecting the deviation in count rates from this initial state measured in time intervals of one second.

By comparing the results from the model simulation using both idealized (synthetic) Poisson and stochastic data with real experimental results, the position of the radioactive source could be determined with an average accuracy of one foot within a 150 ft^2 area. The most impressive feature of this method however, is its ability to be conducted in real time. The model simulations produce single-point localization estimates for the radioactive source at a rate greater than that of the average sampling time of the radiation detectors (1 s). In a real-life situation where an

identified source (i.e. a dirty bomb) is being transported by a person, the pathway taken by the transporter could potentially be observed, aiding with mitigating security risks. However, the algorithm assumes a source of known intensity in order to establish the initial state on which the tracking algorithm is based, meaning that for security applications this would need to be established first to produce similar results; this seems an unlikely scenario within a security threat. The author does, however, state that the algorithm should be part of a 'suite' of tools to help automate the process of detecting security threats, rather than a stand-alone solution. Furthermore, this algorithm requires a network of sensors to interact with radiation levels in excess of background levels to be successful, which may experience detection-limit problems within larger study areas or environments with greater attenuation coefficients than exhibited within the test environment (crowded areas for example). Future work to improve this method should focus on upscaling the size and complexity of the study area to determine impacts on the computational performance of the algorithm and its suitability for realistic security situations.

4.2.2. *RBE algorithms*

A number of studies have explored the use of RBE algorithms in localizing radiation sources (Brennan, Mielke, and Torney 2005; Brewer 2009; Gunatilaka, Ristic, and Gailis 2007; Morelande, Ristic, and Gunatilaka 2007; Muske and Howse 2001; Towler, Krawiec, and Kochersberger 2012). This type of algorithm operates by predicting the behaviour of a system based upon a predefined process model and refining this prediction as new measurements become available. Provided that the process model is representative of the system and the measurements are relatively unclouded by noise, the algorithm converges upon a single probability density function that describes the state of the system (Brennan, Mielke, and Torney 2005; Brewer 2009; Gunatilaka, Ristic, and Gailis 2007; Morelande, Ristic, and Gunatilaka 2007). In terms of localizing a radiation source, this probability density function describes the most likely location for a particular source within the study area.

One of the major advantages of using RBE algorithms is their inherent adaptability to model different dynamical systems (source conditions) and be rewritten to consider a multitude of new measurements that maximize the new available information (Brewer 2009). As such, there are a number of variations of RBE algorithms that are adapted to modelling a range of system complexities (Kalman filter (KF), extended Kalman filter (EKF), unscented Kalman filter (UKF), particle filter (PF), grid-based filter (GF), and element-based filter (EF)). The differences between each of these variations is how they represent the 'belief space' of the model (Brewer 2009), where a belief space herein represents the probability distribution of the location of a radiation source throughout the study area. The ability of the algorithm to accurately localize any source is severely impacted by this belief space. For the following section, it must be recalled that radioactive decay is best represented by a nonlinear, Poisson (non-Gaussian) distribution model.

As previously mentioned, without the appropriate process model on which to base the initial state estimation on, the algorithm will not converge and will, therefore, not provide an accurate estimate on source location. Therefore, the variations of RBE algorithms that are incapable of accurately representing highly non-Gaussian and non-linear

processes (KF and EKF) are unsuitable for application to source localization (Brewer 2009; Gunatilaka, Ristic, and Gailis 2007; Towler, Krawiec, and Kochersberger 2012). However, the UKF variation of RBE algorithms has been shown to be able to provide a convergent estimation for the localization of a single radiation source (Gunatilaka, Ristic, and Gailis 2007). It is a development of the KF and EKF, which allows for some non-Gaussian distribution within the parameters of the process model, meaning it is more suitable for modelling radioactive decay (Brewer 2009). However, the algorithm still struggles with highly non-linear processes, as is experienced at lower levels of radiation intensity. As a result, the accuracy of this method is reported to be lower than other methods, particularly MLE algorithms and more complicated RBE filters (GF, EF, and PF) (Brewer 2009; Gunatilaka, Ristic, and Gailis 2007; Morelande, Ristic, and Gunatilaka 2007; Muske and Howse 2001; Towler, Krawiec, and Kochersberger 2012).

It is apparent that modelling radioactive decay using RBE algorithms requires a variation that goes beyond the scope of the basic KF and its developments (EKF and UKF). One such variation is the PF (Brewer 2009; Morelande, Ristic, and Gunatilaka 2007). A PF is a Monte Carlo simulation technique that represents the posterior belief (state estimation) as a series of randomly distributed state samples (or particles), which relate to a hypothesis of the true state of a target system at any one time (Brewer 2009; Morelande, Ristic, and Gunatilaka 2007; Thrun 2002). Each of these particles has an associated weight/importance, which quantifies the confidence of each hypothesis, given by the current knowledge of the system (provided by the incoming measurements) (Brewer 2009). As new measurements become available to the system, the locations and associated weights are re-evaluated until a likely estimate is established.

An example of this is outlined within Brewer (2009). Using an UAV as a platform for the detection system, a PF algorithm is used to locate a single source of known intensity within a search area of 62,500 m^2. To complete this task, the algorithm initially produces a random distribution of particles throughout the study area, with an evenly distributed weight between them (equal to $1/N$, where N is the number of particles). This is the initial condition for the algorithm because the system has no knowledge of where the source is located (other than being present within the search area) and has not yet received any field measurements, so any point is equally likely to be the source location. As the system receives intensity measurements, it calculates the distance between the UAV sensor and each particle, based upon the estimated distance to the source (a predetermined experimental model for the expected counts for a given distance is used to do this). Following this, the algorithm calculates the normalized error (between 1 and −1) for this point based on the distance calculation and multiplies the previous particle weight by this error. This step of the algorithm determines the new weight for a particle given the measurements by the detector. The particles are then redistributed according to their weights and the distance from each other, converging them towards the most likely locations of the source as the process is repeated. As a non-directional radiation detector is utilized, there tends to be two possible source locations (the true estimate and the ghost estimate). By moving at a tangent to the incoming radiation field, the system distinguishes between the two, creating a single most likely location (or zone).

Running the above algorithm using simulated source data, Brewer was able to demonstrate that a single source could be localized within a defined grid area in less

than one minute with a mean accuracy of around four metres. Whilst these results indicate an impressive accuracy and run time, there are certain limitations associated with the assumptions made within the process; namely the amount of information that is known about the source before the experiment begins. In a real world application, the intensity and identity of the radioactive source is unlikely to be a well constrained value and so to be applicable to realistic situations, the algorithm needs to be developed to deal with unknown source conditions. The necessity for a defined search area also could be a problem in the case where reconnaissance flying has not previously undertaken. Without the knowledge on where to define the boundaries of the search area, the algorithm may potentially experience an increase in running time or a loss of accuracy. Brewer qualifies this by stating that the algorithm should be used as a follow up to high altitude reconnaissance flights in order to further investigate areas of interest. Whilst it has been shown to work well for the test conditions, further experiments should be carried out for areas larger than 62,500 m and adaptations made to allow for the localization of multiple sources.

An example of the use of PF methods without the limitation of these prior knowledge constraints is outline within Morelande, Ristic, and Gunatilaka (2007). By assuming no prior information upon the radiation source within the starting conditions of the algorithm, this PF method aimed to estimate the number of sources, their intensity and their position within a given area based on the knowledge that a source (or number of sources) exist within a defined search area. Using an importance sampling method (similar to the particle weighting method used by Brewer) with progressive correction instead of resampling, the authors demonstrate that PF algorithms have the capacity to accurately estimate up to three unknown sources, using either a single mobile sensor or a distributed network of sensors. A Cramer–Rao bound (CRB) analysis is used as a performance indicator to test this algorithm against; also covered within this study is another algorithm (a variant of a MLE), which is covered in the following section.

In a series of repeated simulations, the algorithm was able to successfully identify the number of sources, locate them and estimate their intensity for the majority of cases. All experiments were carried out using an array of 60 sensors arrange in a circle, with a radius of 200 m (approximately 125,660 m^2 area). In terms of estimating the number of sources for a given dataset, the algorithm was exceptional, particularly at identifying one or two sources (100% success rate). When a third source is introduced, the algorithm becomes less reliable at estimating the number of sources (between 81% and 93% success rates at varying signal-to-noise (SNR) ratios), sometimes over-estimating the number of sources present. Even so, these success rates are exceptional, especially considering the decreased running time relative to the MLE also featured within this study. Additionally, the algorithm was able to accurately locate the number of sources even at very low SNR (5 dB) to a degree of accuracy that outperforms even the CRB estimate for a lower bound in some cases. A similar situation is observed for the intensity estimate of the sources.

An alternative to the PF method is the grid-based filter (GF) (Towler, Krawiec, and Kochersberger 2012). This algorithm works by splitting the defined search area into a series of defined grid points rather than representing posterior belief through a series of particles. The advantage of this technique compared to the PF method is that it requires

no tuning of parameters or compensation for problems inherent within the PF method (degeneracy for example). However, this technique ultimately falls short of the PF method presented by Morelande, Ristic, and Gunatilaka (2007), as this GF algorithm becomes significantly more computationally expensive as any dimension of the algorithm is increased (search size, spatial resolution, or number of sources). Moreover, the priory, on which the algorithm is based, requires a known number of sources, isotopes and activities in order to work.

Using a single UAV-hosted sensor, the algorithm creates its prior grid using a uniform distribution model, such that it is equally likely that any location within the grid is source location (the source is placed in a known, but random location, which lies fully within a single grid square). Having established a background radiation intensity for the area, the sensor begins iteratively measuring the radiation level and comparing it to the observed background value. If the measured value is in excess of the background level, then the source is assumed to be detected. The expected number of counts for all grid cells is then computed, based on the assumption that the source lies within the observed cell. The likelihood that the source exists within this cell is the probability that this obeys a Poisson distribution about a mean corresponding to the expected number of counts from that cell. The algorithm will continue to iterate (moving the sensor between each iteration) until this probability has reached a threshold of 90%, which is described as the condition for 'complete localization' of the source (Towler, Krawiec, and Kochersberger 2012). In the case where the measured counts is equal to or lower than the background level for the area, the source is assumed to not be present within the detectable range of the sensor and so the likelihood that source is within this range is determined to be low/zero. The algorithm therefore updates the prior belief according to this observation. Similarly to the motion control used within Brewer (2009), as the sensor converges upon the likely location, it moves orthogonally to the incoming radiation field (at a tangent), so as to distinguish ghost estimates from the true source location.

Whilst the limitations relating to the requirement for known source conditions hold back this algorithm in comparison to other available filters, the performance of this algorithm under the simulation conditions is exceptional. In nearly 1200 realizations, the algorithm took no more than 38 iterations, from the point of detection, to completely localize the source. Considering the rate at which these iterations occur (1 Hz), the authors state that the algorithm will take no more than approximately 30 s to localize a source after the initial detection. Moreover, given that the source lies completely within a grid cell, the error on the localization calculation will correspond to the resolution of the grid cell at the point of 90% confidence. This has the implication that at 'complete localization' within a grid of cells measuring one square meter in area, the error on the localization calculation will be 1 m. Hence, this algorithm presents an exceptional performance in this capacity. However, this error will increase with an increase in the size of each grid cell.

Comparing the available RBE algorithms, it seems that the PF variations, particularly the method outlined within Morelande, Ristic, and Gunatilaka (2007), offer the most potential for localizing radiation sources in real-life situations. These variations currently provide the best compromise between the ability of an algorithm to represent the highly non-linear and non-Gaussian nature of radioactive decay and the required computational expense (equivalent to algorithm running time) (Brewer 2009). In all

cases, they outperform the various Kalman filter algorithms and do not suffer from the same 'curse of dimensionality' that the GF and EF versions of RBE algorithms experience as search parameters increase in magnitude (Towler, Krawiec, and Kochersberger 2012). Furthermore, the PF remains the only variation to have been shown to perform well when there is little known information on the source before the algorithm begins.

4.2.3. *MLE algorithms*

The MLE algorithms (Gunatilaka, Ristic, and Gailis 2007; Morelande, Ristic, and Gunatilaka 2007) differ from the Bayesian and other algorithms outlined above as no prior information (other than the number of sources) is required on the radiological source before the procedure begins (Gunatilaka, Ristic, and Gailis 2007; Morelande, Ristic, and Gunatilaka 2007; Towler, Krawiec, and Kochersberger 2012). An MLE algorithm is a block algorithm that estimates parameters for a given dataset provided that; the dataset is large enough, the measurements within the dataset are mutually independent of each other and an unbiased minimum variance estimator exists for the dataset. The output of the algorithm is a vector which maximizes a given likelihood function (provides the most likely result) (Gunatilaka, Ristic, and Gailis 2007; Morelande, Ristic, and Gunatilaka 2007). Within radioactive source localization, this vector describes the most likely location of a particular radioactive source within a given area.

Based on the assumption that the number of sources is known, Gunatilaka, Ristic, and Gailis (2007) used an MLE algorithm to localize a single point source successfully. The method was tested against a CRB analysis of idealized laboratory data, which provides a lower bound value for the estimation accuracy of a desired parameter (Gunatilaka, Ristic, and Gailis 2007; Morelande, Ristic, and Gunatilaka 2007). The method was also tested against EKF and UKF Bayesian algorithms. Whilst the algorithm is more computationally expensive than the comparative Bayesian algorithms (as it stores and considers all previous measurements within every iteration, rather than representing these within a posterior belief function [Brewer 2009; Gunatilaka, Ristic, and Gailis 2007]), the authors concluded that the MLE method provided the most accurate localization estimate (closest to the CRB estimate), as the value continually converged towards the CRB value as the dataset size increased. At small dataset values however (less than 33 entries), the parameters could not be accurately estimated as the algorithm is driven unstable without enough data to iterate through.

Whilst Gunatilaka, Ristic, and Gailis (2007) concluded that the MLE algorithm outperformed the EKF and UKF algorithms at confidently localizing a radiation source, further work within Morelande, Ristic, and Gunatilaka (2007) posed a new situation to be investigated. In this study, the MLE algorithm was used to identify multiple sources within a target error whilst keeping the number of sources within an area as an unknown variable. As the MLE algorithm assumes the number of sources to be a predefined value, the algorithm outlined within Gunatilaka, Ristic, and Gailis (2007) was insufficient in its original form to complete this task. A model order selection process using the general maximum likelihood (ML) rule was used to estimate the number of sources present from a given dataset before determining their location. This modification allowed the MLE parameter estimation to iteratively occur for a hypothesized number of individual sources (zero to a maximum specified value (r)) and determine the most likely situation for a given dataset. Similarly to Gunatilaka,

Ristic, and Gailis (2007), this method was tested against a RBE algorithm (albeit a better adapted version for non-linear Gaussian problems than the EKF and UKF variants tested in Gunatilaka, Ristic, and Gailis [2007] and a CRB analysis to determine its performance.

In an exhaustive test, in which 100 individual iterations of a simulation was run for zero, one, and two sources in the presence of simulated noise (SNR of 10, 15, and 20 dB), this method was able to correctly identify two sources within a scenario in 95% of the iterations for an SNR of 15 dB and 97% of the iterations for an SNR of 20 dB. However, in the presence of relatively high noise (SNR of 10 dB), the ability of the algorithm to detect more than a single source was greatly reduced to 68% of the iterations. This creates concern over the ability of the algorithm to perform in real world applications (where SNR is often low), for example; where source strength may be only be slightly in excess of background levels, the study area is larger than that used within the test or where the survey environment is more complicated than the simple scenario tested (for instance a crowded room). In a realistic scenario, where an unaccounted radiological security threat is present, an unobstructed room is highly unlikely to be the featured environment. Therefore, further testing of this algorithm in these situations is pertinent before it is further implemented. Most importantly, however, the computational requirements of this algorithm for more than two individual sources are vast; during the testing of the algorithm for three sources, the authors were unable to establish a reasonable run time. Therefore, for a situation where more than two sources are suspected, a different algorithm is required.

4.2.4. *Contour mapping algorithm*

In addition to the RBE and MLE algorithms featured in the work of Morelande, Ristic, and Gunatilaka (2007), the contour mapping localization algorithm provided by Towler, Krawiec, and Kochersberger (2012) assumes no prior knowledge on any characteristic of the radiation source or the number of sources present within an area. Using a mapping approach to localization, the authors attempt to identify point sources with the intention of using this to identify hazardous regions following large radionuclide releases into the environment. By assuming that air is a homogeneous medium, it can be defined that the intensity contours from a single emitter form concentric spheres with the intensity decreasing outwards from the centre. By tracing the entire length of a specific contour, the location of the point source can be determined to lie at the centre of this circle. Additionally, as the distance to the centre of the circle and the intensity of the flight path are known, the intensity of the source can be estimated according to Equation (2). In the case of multiple sources, the shape of the contour will change predictably according to the interaction between the level curves produced from each source. The full algorithm is separated into three stages: contour detection, contour following, and source localization.

The first step (contour detection) aims to rapidly establish a user defined intensity contour following the identification of a point source within a given area. As the authors intend this algorithm to be utilized within time pressured situations (for example security-sensitive or post-disaster environments), this step is optimized to perform as efficiently as possible, with the airborne platform moving at the greatest possible velocity in a time efficient Archimedean spiral pattern over the area. The search ends when the desired contour is detected. Following the identification of the target contour,

the system begins to autonomously follow the contour, in a counter-clockwise direction at a reduced velocity (6–15 m s^{-1}), using detection limit of $\lambda_d + \lambda_d^{0.5}$(where λ_d is the desired contour). This limit ensures that the system is always following the inside of the contour until the entire contour is mapped for the study area.

Following the completion of the contour mapping process, the position and recorded intensity of every point mapped by the UAV system are extracted and plotted as a 2D plan view of the site. The plot is then converted to a binary image and a Hough transform applied. This feature extraction technique identifies line patterns within an image, allowing it to be implemented to find curves/circles that are inferred by lines present within the image (Shapiro and Stockman 2001). Towler, Krawiec, and Kochersberger (2012) use this transform to provide estimates on the position of the centre of the circles based on the traced intensity contour from the mapping results (both idealized and stochastic tests). As this transform returns a number of estimates, invalid candidates (those estimates, which lie outside the circle) are removed and confidence estimates are used to eliminate all but the most likely centre positions from the remaining candidates. The intensity of the source is then calculated using an adapted form of Equation (2). In the case of multiple sources, which interact with each other, the intensity is iteratively calculated using multiple points along the mapped contour until the estimates converge.

Using this approach, the authors were able to localize up to three radiation sources with a mean position error of 17.86 m in the more realistic stochastic simulations. Whilst this seems less accurate than the other methods outlined in this section, this is not necessarily the case upon detailed inspection. First, the contour mapping algorithm requires no prior information specific to the radiation source; only the definition of what intensity contour to follow. Whilst this does require the operator to know something about the general activity of the site's radiation, it is much easier to obtain when compared to other methods, which require more specific inputs such as the number of sources (Brennan, Mielke, and Torney 2005; Brewer 2009; Howse, Ticknor, and Muske 2001; Towler, Krawiec, and Kochersberger 2012), isotope present (Howse, Ticknor, and Muske 2001; Towler, Krawiec, and Kochersberger 2012), or the actual intensity (Brewer 2009; Howse, Ticknor, and Muske 2001). Moreover, whilst other methods (for example, the RBE method from Towler, Krawiec, and Kochersberger [2012] and the combined MLE/ML algorithm from Morelande, Ristic, and Gunatilaka [2007]) may suffer from a 'curse of dimensionality' (Towler, Krawiec, and Kochersberger 2012), the contour mapping method does not encounter this problem. This method was tested this in a 1 km^2 field; the largest by far in any of the aforementioned studies. By considering this area in relation to its mean position error and lack of prior information, the presented accuracy is good. Therefore, this presents little concern over its ability to upscale to larger areas, making it more suitable for larger-scale operations such as rapidly identifying areas of risk following a large radionuclide release.

There are, however, a number of limitations associated with the use of this algorithm to localize an unknown number of sources. One such problem arises when there is a source of high intensity proximal to low intensity sources. In this case, masking of the lower intensity sources by the higher intensity source can occur to the point where the lower intensity source is undetectable within the intensity ring of the higher intensity source (Towler, Krawiec, and Kochersberger 2012). Whilst efforts to establish localized

hazardous regions in this case would not be affected too badly, it means that the adaptability of the algorithm to identify all sources in an area is implicated. A method to reduce this impact would be to reduce the flight altitude (which would theoretically also decrease the positional error), although this would increase the time taken to complete the survey. As the authors suggest the time efficiency of the technique is one of its advantages, this may not be preferred for some applications.

A further limitation that can be identified within the stochastic simulation results is the identification of 'ghost' sources. These arise from variations within the measured count during the contour following step of the algorithm. As the system detects radiation over an integration period of one second (Towler, Krawiec, and Kochersberger 2012), it responds to variations in the measured intensity by altering its flight path to continue mapping the desired contour. The variations within the stochastic simulation caused the flight path to vary wildly from a perfect circle (as in the idealized simulation), which are interpreted in some cases as small point sources within the Hough transformation during the localization part of the algorithm. Assuming no prior knowledge of the area, these would have to be further investigated to discount them as sources, although their location on the edge of the traced contour might identify them as spurious.

Overall, this algorithm represents a simpler, more computationally efficient method of localizing stationary radiological sources than the other methods outlined within this section. Whilst the average error is larger than other methods, particularly that of the PF/GF, RBE, and MLE algorithms (Brewer 2009; Gunatilaka, Ristic, and Gailis 2007; Morelande, Ristic, and Gunatilaka 2007; Towler, Krawiec, and Kochersberger 2012), this method seems to have no upper bound in the number of sources it can be applied to (provided that they are distinguishable from each other at the operational altitude). The overall choice of algorithm, however, depends entirely upon the intended aim of any particular application or study. In the case of rapidly identifying numerous unknown sources following a large-scale nuclear release, then the mapping-based algorithm from the work of Towler, Krawiec, and Kochersberger (2012) currently seems like the most appropriate choice. However, if some information is known on the source characteristics and search area, then various Bayesian methods provide more accurate and temporally efficient methods of producing localization estimates.

5. Radiation attenuation in radiometric surveys

As described in the articles by Sanderson et al. (1995) and MacFarlane et al. (2014), the altitude of the survey flight influences the measured intensity according to the inverse square law. In addition to this is the lesser effect of radiation attenuation by water and other gaseous components within the air. In radiation surveys, the effect of radiation attenuation acts to further reduce the amount of radiation detected. Surveys carried out by handheld ground-based methods are associated with an intrinsic attenuation through human–radiation interactions, which can incur a reduction of 30–35% of the actual intensity (Jones and Cunningham 1983). This reduction, however, is a general value for a human male pertaining to an average calculated from experimental data and meaning that currently no comprehensive method exists for determining actual attenuation occurring from a specific operator. By using an aerial platform, this reduction is

completely avoided, allowing for well constrained corrections of the output data to a normalized dose rate at a specific height (typically 1 m [Martin et al. 2015; Sanada and Torii 2015]).

Gamma ray attenuation can be described as the reduction of radiation intensity by the interaction of the electromagnetic ray with the atoms of the material it is propagating through. Mathematically, this can be described for a homogeneous absorber as follows:

$$I = I_0 e^{-(\mu \rho x)}, \tag{3}$$

where I_0 represents the incident ray of a given energy with no attenuation, I, the intensity of attenuated ray after passing through the material, μ, the mass attenuation coefficient ($cm^2\ g^{-1}$), ρ, the density ($g\ cm^{-3}$) and x, the thickness of the material (cm) (Davidson, Biggar, and Nielsen 1963; Grodstein 1957a; Hubbell 1969; Leclair 2010). The mass attenuation coefficient is a combination of the linear attenuation coefficient (cm^{-1}) and the density of the material ($g\ cm^{-3}$). Attenuation occurs through a number of methods, detailed earlier, including different types of absorption and scattering (Davidson, Biggar, and Nielsen 1963; Grodstein 1957a; Hubbell 1969). At low photon energies the photoelectric effect is the main contributor (approximately 80%) to attenuation. This effect can be seen to have an increasing probability with increased Z number (Figure 3). Also acting at these energies is the process of Rayleigh scattering (Grodstein 1957a; Hubbell 1969). At higher photon energies (0.5–5.0 MeV), Compton scattering becomes the most dominant process. Above 1 MeV, absorption of the photon by the nucleus can occur to produce a positron/electron pair emission. This process increases in probability with increasing photon energies up to around 25 MeV (Grodstein 1957a) becoming the dominant form a very high photon energies, though this would not typically be relevant to either environmental or industrial radiation monitoring.

It can be seen in results from Grodstein (1957b) and Hubbell (1969) that water within air has a greater effect upon attenuation that dry air. It is therefore appropriate to consider the amount of water within the air as a factor of the attenuation properties of air. This attenuation is shown graphically in Figure 4. Comparing the attenuation curves from the theoretical humidity curves and previous works on radiation detection, it can be seen that there is little to no effect from the humidity of the air, as water makes up a very small weight percentage of the constituents (around 0.015 $kg\ m^{-3}$). The dominant factor on the reduction in radiation intensity can therefore be considered to be geometric spreading.

Although humidity has little effect on attenuation, precipitation (rain or fog) is likely to have a larger effect. This arises from the increased concentration of water per unit volume of air that can be attained by precipitation. Furthermore, airborne particulates are likely to be of importance due to their large density contrast with respect to air and water. It is therefore necessary to quantify the particulate concentration in areas of the world where it is likely to be a problem. There is however added complexity due to the large number of chemical components that can make up any airborne particulate compared to the two-component system assumed in the humidity calculation. Particulates within the atmosphere are of greatest importance in

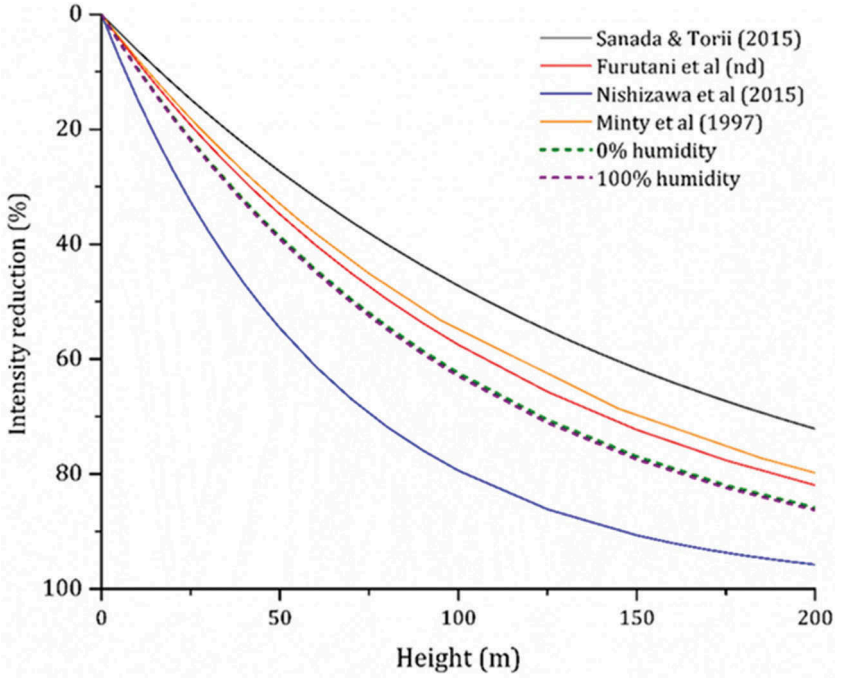

Figure 4. Attenuation curves from four previous airborne studies shown in comparison to the theoretical attenuation effects of humidity.

areas of high pollution (e.g. urban smog) or in arid areas with little in the way of vegetation to hold loose soil and sand particles on the ground, resulting in frequent dust storms. Constituents of modern urban smog occurrences are mostly SO_2, NO_X, CO, and respirable particles (Fenger 1999; He, Huo, and Zhang 2002) and are typically much higher Z number than water, meaning that an increase in the proportion of these constituents within a given air packet would have a greater attenuation effect than an increase in humidity for a given value. In calculating the attenuation by an air packet rich in particulates, a constraint on the constituents of the particulates would have to be estimated or measured. Kurvinen et al. (2005) employed the use of an air sampling unit integrated into the payload which would provide a potential solution to this problem, allowing for the determination of the particulate content of the air through testing once the survey is complete. It must be taken into account, however, that this study used a UAV that had a much larger payload (45 kg) than any other following studies, allowing for the incorporation of many different elements to the payload. Other studies may experience problems due to weight restrictions such additions may not be practical for a smaller UAVs, but this data may instead be sourced via satellites, weather radar or ground based particle sampling units (Engel-Cox, Hoff, and Haymet 2012).

Quantifying the air particulate concentration is useful in a number of ways. As air particles act to increase the attenuation of radiation, the knowledge could be used to add corrections to data collected by airborne surveys to increase the accuracy of the overall results. Moreover, when identifying point sources in a situation with multiple

sources in one area, high particulate concentration or heavy precipitation can actually aid to improve the accuracy of identifying each individual point source by minimizing the crossover of emitted radiation from each point source. This would, however, not be the case in the event of a radioactive plume.

6. 3D visualization as a tool for improving radiation surveys

The current method for visualizing the results from radiometric surveys comprises of overlaying a colour-scaled intensity map onto a two dimensional satellite image. Whilst this gives a good representation of the hotspot locations, it imparts limited information on the relationship of these hotspots to the surface features. By overlaying radiation maps onto 3D surface models, the relationship between the radiation distribution and the topographic surface can be more confidently constrained. This would provide a useful analytical tool to more successfully inform management strategies should they be necessary. For example, such an approach could more efficiently identify radiation shine paths for intense emitters in areas for example high/intermediate level nuclear waste storage facilities.

The construction of these maps can be achieved through the use of GIS software; comprising a 3D surface model and a colour-scaled radiation intensity overlay. The 3D surface model can be constructed using a DEM (either in a raster or ASCII format) as a starting point and converting this into a triangular irregular network (TIN). A TIN represents the topography as a series of irregular triangles, which form a 3D surface with the vertices of the triangles corresponding to the referenced data points within the metafile. There are a number of methods with which to obtain a DEM. First, there are a number of free-to-download files available (for example, ASTER-GDEM, SRTM, or Digimap™ (UK)), although these tend to be limited in terms of their spatial resolution. For example, the Digimap™ service, provided by Ordnance Survey (OS) UK, offers data files tailored for use within GIS software, including DEM files (up to 5 m resolution), geological data, and map data (Ordnance Survey (GB) 2015).

As an alternative to the relatively low resolution of the free-to-download DEM data, there are a number of methods available for obtaining DEM data at much higher resolutions (up to millimetre scale accuracy). Two viable methods are discussed herein; lidar and various photogrammetric methods.

6.1. *Lidar and radiometric surveys*

Understanding position, but importantly height above the ground is highly important for accurate airborne radiation mapping. Whilst barometry can provide altitude based on atmospheric pressure, laser ranging provides a more precise technological alternative to provide height above the ground to within centimetre or even millimetre accuracy. Lidar is defined as an 'optics remote sensing technology that measures properties of scattered and reflected light to find range and/or other information about a distant target' (Karp and Stotts 2012). Modern systems use the 'time of flight' method (Figure 5) to measure the distance to the target surface (Glennie et al. 2013; Karp and Stotts 2012; Stefanik et al. 2013). There are two variations of the technology to consider for radiation mapping applications: (i) single point range finders and (ii) 3D scanning systems.

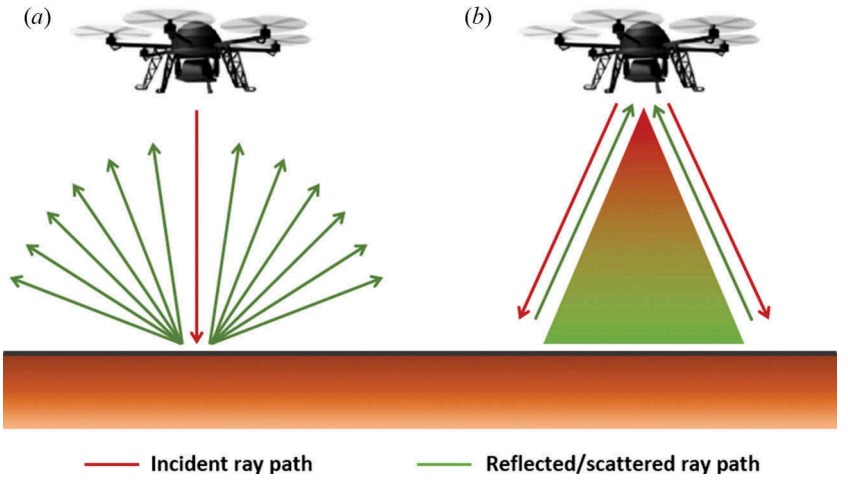

Figure 5. Illustrative comparison of (*a*) pulse (single-point range-finder systems) and (*b*) 3D-scanning laser systems.

A single point range finding system uses discrete pulses of light at the rate of a few nanoseconds per pulse at a specific wavelength and energy. Reflectance from the emitted beams hitting surfaces returns to the system where they are detected and the distance is calculated. A 3D scanning system works in a similar way, but uses a beam dispersal attachment (often an oscillating block or rotating mirror) to divert the emitted beams in multiple directions to create a 'beam swathe' (Figure 5). Using this swathe combined with the physical movement of the system across a target area, a 3D point cloud can be produced, which can be processed into a 3D representation of the area (Glennie et al. 2013; Stefanik et al. 2013). The length of the laser pulses in both variations produces a minimum length for the observation beam; causing issues with overlapping reflections at distances smaller than the beam length. For example, the situation described in the article by Glennie et al. (2013) details that a 10 ns pulse duration corresponds to a 3 m path length, hence a target within this range will be poorly represented.

Both variations of the lidar systems can be utilized on ground and mobile platforms, and have been extensively used in numerous studies across a range of applications including detailed geological mapping, site surveying, and crime scene investigation.

6.1.1. *Single point range finding systems*

MacFarlane et al. (2014) and Martin et al. (2015) used a single point range-finder on a gyro-stabilized as part of the unit's payload for accurate height above ground measurements (±10 mm at <100 m) (AR2500 Acuity^{TM}, n.d.) to improve the quality of the radiation intensity data. The advantage of this system is that radiation/dose data can be accurately normalized for height at every individual data point throughout the survey, reducing calculation uncertainty by providing a definitive error associated with the reading, rather than a general normalization associated with flying at a particular altitude without using a lidar.

During lidar surveys, the emitted beam undergoes a combination of backscattering from constituents within the ray path (e.g. water and other gaseous molecules within air) as well as diffuse and secular scattering from reflective surfaces (Figure 5), these former factors act to attenuate the strength of the returning signal. The electrical systems of the computer can distinguish the signals using the leading edge detection of the returning beam relative to the incident (Glennie et al. 2013; Karp and Stotts 2012). Edge detection is the algorithm used by the system to detect the returning signal by looking for sharp changes in the signal characteristics received by the sensor relative to the background. Leading edge detection is a variant of this, where the sensor detects sharp changes in the signal resulting from the detection of the first arrival of the returning signal (Sharp, Yu, and Guo 2009). MacFarlane et al. (2014) and Martin et al. (2015) overcame the problem of secular scattering to a large extent by orientating the detection equipment upon a gyroscopic platform, with the single point range-finder pointing normal to the surface. The effect of diffusive scattering is also not a significant limitation; the low altitude of the flight intercepts the scattered region early compared to higher altitudes. In reality, the roughness of the ground and the influence of topography will produce more secular and diffusive scattering than the flat Lambertian surface shown in Figure 5, however, the results are unlikely to be affected strongly by this as the signal strength is large at emission, hence a large proportion still returns to the detector (Glennie et al. 2013).

Similarly, there may well be a number of reflective surfaces within the ray paths that create more than one reflection or stop the beam from reflecting off the target surface before returning back to the detector. This has the result of lengthening or shortening the recorded distance. Within radiation mapping, the target surface is usually the ground surface or the surface of buildings on which radioactive fallout can reside. As a result, vegetation acts as the problematic reflective surface, especially in regions surrounding Fukushima, where vegetation has remained untouched since the incident. However, this can be overcome by looking at the edge detection of the last response of the reflected beam rather than the first, allowing the ranging measurement to be tuned to ignore vegetation.

6.1.2. *3D scanning systems*

The results from MacFarlane et al. (2014) and Martin et al. (2015) show that the use of lidar within UAV radiation surveys is an effective method to reduce uncertainty within the calculated radiation intensities. However, the scope of lidar usage should not be limited solely to altitude measurements. The incorporation of 3D scanning lidar with reference to radiation mapping has been overlooked to date. The inclusion of this technology enables the production of highly accurate 3D DEMs as an additional analytical tool, allowing for more accurate representations of radiation distribution in an area.

6.2. *Photogrammetry and stereovision*

Photogrammetry and stereovision techniques may also be used to extract 3D information from a ground surface (Stefanik et al. 2013). Photogrammetry uses a single moving camera to create a sequence of overlapping images. Each of the images are then combined using correlated focal points and image matching algorithms to produce a three dimensional image of the area (Stefanik et al. 2013). This is the most common method of producing

three dimensional reconstructions of an area with an accuracy of 10–90 cm both horizontally and vertically (Grenzdörffer, Engel, and Teichert 2008), although recent unpublished work within the University of Bristol has been able to obtain spatial resolutions of around 5 cm both horizontally and vertically from a flight altitude of 70 m. Stereovision (Sanada and Torii 2015) works using similar principles to photogrammetry, but uses two rigidly affixed cameras at different angles to the surface from each other to take photographs of the environment. The camera's shutters are synchronized by the carrying system to ensure that photographs are taken at the same time and that the motion of the carrying system does not affect the calibration (Stefanik et al. 2013). A major problem with the use of photogrammetry is that the technique is not suited for imaging dynamic environments such as those with moving traffic or trees blowing in the wind as the method assumes a static environment (Stefanik et al. 2013). Stereovision does not experience this problem and unlike photogrammetry and lidar methods, can extract 3D information from the combined image without the need for physical movement of the system.

Stefanik et al. (2013) provides a comparison of all three methods (lidar, stereovision, and photogrammetry) alongside outlining the performance of a UAV stereovision system using a Yamaha RMAX platform. The conclusions from Stefanik et al. (2013) confirm that both stereovision and lidar scanning systems are suitable methods to produce three dimensional reconstructions using a UAV. The two methods however, are advantageous in different ways. Lidar scanning systems have a high accuracy and constant systematic error associated with the 'time of flight' workings of the system, which is independent of the distance from the target surface. In contrast, stereovision systems display an error increasing in a quadratic function with distance from the target, but can display a higher accuracy compared to the lidar system used in the study at low altitudes. A further advantage for stereovision is the acquisition of textural data during the survey, whereas lidar systems require much more processing and analysis of the returned beam intensity in order to extract textural information. Even in the case where this is possible, the extracted textural data may be ambiguous in comparison with the photogrammetry techniques.

Stefanik et al. (2013) state that with the inertial movement of the lidar scanner to produce the 3D view, the accumulated error of the measurements increases relative to if the scanner were to remain stationary. This could potentially be a factor in the lower accuracy compared to the stereovision system at low altitude. By finding a way to decrease this it might be possible to further reduce the systematic error associated with the lidar scanner. Overall, the study concludes that lidar presents the best solution for three dimensional imaging at higher altitudes and in areas where topography is variable, whereas stereovision has a better accuracy at low altitudes and uses much less power and weight as part of the payload. Currently, there has been no published works on the usage of 3D scanning lidar in conjunction with UAV radiation mapping, whereas stereovision has been used as part of Towler, Krawiec, and Kochersberger (2012). This study used the system to produce terrain maps of areas of interest (hotspots) to allow for more accurate inference into the nature of the distribution of radioactivity within the area. Possible additions to the scope of this technology in the future will be to look at producing three dimensional models for sites of complex geometry, e.g. nuclear waste storage and reprocessing facilities, where the combined radiation and 3D scanning survey data can be used to make an inverse calculation of the true radiation field for the purposes of identifying unexpected shine paths or radiation originating from buildings, not just the ground surface.

7. Conclusion

There can be no doubt that the use of UAVs to carry out radiation surveys is an invaluable tool in furthering the efficiency of the response to future nuclear accidents and disasters. The technique has the capability to produce high resolution maps without the need to endanger workers or incur great expense. The data acquired from these systems can be used to aid policy, mitigation and management plans for potential nuclear disasters in the future as well as be adopted for routine use in day-to-day site monitoring, scanning of cargo ships, vehicles, and even the identification of certain ore deposits based on their characteristic radiological signatures.

Early works from before the Fukushima incident in 2011 (Kurvinen et al. 2005; Pöllänen et al. 2009) tested the feasibility of different systems in detecting radiation using fixed-wing UAVs of different sizes and in different scenarios. The studies identified the necessity for unmanned systems when it comes to localizing or mapping potentially harmful radiation levels as it dramatically reduces the risk and/or time associated with the acquisition of data through manned methods.

In the aftermath of the Fukushima incident, there was a notable increase in the number of studies relating to UAV-based radiation detection (Furutani et al., n.d.; MacFarlane et al. 2014; Martin et al. 2015; Sanada and Torii 2015; Towler, Krawiec, and Kochersberger 2012). The UAV systems outlined in these studies displayed numerous detector systems and mapping solutions. The choice of system will be strongly dependent upon the task to be completed, as differing systems present strongly contrasting benefits and limitations as highlighted. The growing body of data clearly highlights the increased spatial resolution and sensitivity that can be provided by low altitude UAV surveys relative to the higher altitude methods previously deployed, although this comes at a loss of temporal coverage. Certain publications in the recent past (MacFarlane et al. 2014; Martin et al. 2015; Towler, Krawiec, and Kochersberger 2012) have included additions to the payload to enhance the data collection and presentation. Single point range-finding lidar systems have been shown to increase the accuracy of the altitude determination of the sensor, leading to reduced uncertainty in the radiation level data. Moreover, the use of stereovision (Towler, Krawiec, and Kochersberger 2012) has also been shown to produce combined terrain maps of areas of interest to the operator, allowing for targeted improvements on the spatial distribution of radioactivity, important for aiding clean-up and management strategies following a nuclear release event.

Future developments of these systems should look to produce accurate three dimensional models of radiation distribution. The use of stereovision and 'structure from motion' as outlined in the work of Stefanik et al. (2013), as well as 3D-scanning lidar provide promising methods for achieving this vision. Future studies should look to further identify the advantages/disadvantages of each of the respective systems and compare the practical uses of a range of systems and algorithms that are available to use.

Disclosure statement

No potential conflict of interest was reported by the authors.

Funding

This work was supported by the Engineering and Physical Sciences Research Council [EP/K503824/1].

ORCID

P. G. Martin http://orcid.org/0000-0003-3395-8656

References

AR2500 Acuity™. n.d. *Acuity AR2500 Specification*. Accessed 02 November 2016. http://www.acuitylaser.com/products/item/ar2500-laser-sensor

Bolsunovsky, A., and D. Dementyev. 2011. "Evidence of the Radioactive Fallout in the Center of Asia (Russia) following the Fukushima Nuclear Accident." *Journal of Environmental Radioactivity* 102 (11): 1062–1064. doi:10.1016/j.jenvrad.2011.06.007.

Boudergui, K., F. Carrel, T. Domenech, N. Guenard, J.-P. Poli, A. Ravet, … R. Woo. 2011. "Development of a Drone Equipped with Optimized Sensors for Nuclear and Radiological Risk Characterization." In *2011 2nd International Conference on Advancements in Nuclear Instrumentation, Measurement Methods and Their Applications*, 1–9. doi:10.1109/ANIMMA.2011.6172936.

Brennan, S. M., A. M. Mielke, and D. C. Torney. 2005. "Radioactive Source Detection by Sensor Networks." *IEEE Transactions on Nuclear Science* 52 (3): 813–819. doi:10.1109/TNS.2005.850487.

Brewer, E. T. 2009. *Autonomous Localization of 1/R^2 Sources Using an Aerial Platform*. Virginia Tech. https://vtechworks.lib.vt.edu/handle/10919/36378

Buchanan, E., A. J. Cresswell, B. Seitz, and D. C. W. Sanderson. 2016. "Operator Related Attenuation Effects in Radiometric Surveys." *Radiation Measurements* 86: 24–31. doi:10.1016/j.radmeas.2015.12.029.

Buesseler, K., M. Aoyama, and M. Fukasawa. 2011. "Impacts of the Fukushima Nuclear Power Plants on Marine Radioactivity." *Environmental Science & Technology* 45 (23): 9931–9935. doi:10.1021/es202816c.

CAA. 2015. Small Unmanned Aircraft: Specific Regulations about Small Drones. Accessed January 29 2016. https://www.caa.co.uk/Commercial-industry/Aircraft/Unmanned-aircraft/Small-unmanned-aircraft/

Canberra. 2014. *Gamma and X-Ray Detection*. http://www.canberra.com/literature/fundamental-principles/pdf/Gamma-Xray-Detection.pdf

Cao, Y., X.-B. Tang, P. Wang, J. Meng, X. Huang, L.-S. Wen, and D. Chen. 2015. "Spectrum Correction Algorithm for Detectors in Airborne Radioactivity Monitoring Equipment NH-UAV Based on a Ratio Processing Method." *Nuclear Instruments and Methods in Physics Research Section A: Accelerators, Spectrometers, Detectors and Associated Equipment* 797: 290–296. doi:10.1016/j.nima.2015.07.012.

Chen, H., S. A. Awadalla, F. Harris, P. Lu, R. Redden, G. Bindley, A. Copete, et al. 2008. "Spectral Response of THM Grown CdZnTe Crystals." *IEEE Transactions on Nuclear Science* 55 (3): 1567–1572. doi:10.1109/TNS.2008.924089.

Davidson, J. M., T. W. Biggar, and D. R. Nielsen. 1963. "Gamma-Radiation Attenuation for Measuring Bulk Density and Transient Water Flow in Porous Materials." *Journal of Geophysical Research* 68 (16): 4777–4783. http://onlinelibrary.wiley.com/doi/10.1029/JZ068i016p04777/pdf

Engel-Cox, J. A., R. M. Hoff, and A. D. J. Haymet. 2012. "Recommendations on the Use of Satellite Remote-Sensing Data for Urban Air Quality." *Journal of the Air & Waste Management Association*. doi:10.1080/10473289.2004.10471005.

Fenger, J. 1999. "Urban Air Quality." *Atmospheric Environment* 33 (29): 4877–4900. doi:10.1016/S1352-2310(99)00290-3.

Furutani, T., K. Uehara, K. Tanji, M. Usami, and T. Asano. n.d. "A Study on Micro-Scale Airborne Radiation Moni-toring by Unmanned Aerial Vehicle for Rural Area Reform Contaminated by Radiation." no. 1: 1–9. http://www.ists.co.jp/wordpress_en/wp-content/uploads/Study-report.pdf

Glennie, C. L., W. E. Carter, R. L. Shrestha, and W. E. Dietrich. 2013. "Geodetic Imaging with Airborne Lidar: The Earth's Surface Revealed." *Reports on Progress in Physics. Physical Society (Great Britain)* 76 (8): 086801. doi:10.1088/0034-4885/76/8/086801.

Green, A. A. 1987. "Leveling Airborne Gamma-Radiation Data Using Between-Channel Correlation Information." *Geophysics* 52 (11): 1557–1562. doi:10.1190/1.1442272.

Grenzdörffer, G., A. Engel, and B. Teichert. 2008. The Photogrammetric Potential of Low-Cost Uavs in Forestry and Agriculture. *The International Archives of the …*. http://www.isprs.org/proceedings/XXXVII/congress/1_pdf/206.pdf

Grodstein, G. 1957a. X-Ray Attenuation Coefficients from 10 Kev to 100 Mev. *NBS Circular, 583*. http://oai.dtic.mil/oai/oai?verb=getRecord&metadataPrefix=html&identifier=ADA278139

Grodstein, G. W. 1957b. "X-Ray Attenuation Coefficients from 100 Kev to 100 Mev." *National Bureau of Standards Circular* 583 (583): 1–58.

Gunatilaka, A., B. Ristic, and R. Gailis. 2007. "On Localisation of a Radiological Point Source." In *2007 Information, Decision and Control*, 236–241. IEEE. doi:10.1109/IDC.2007.374556.

Guss, P. 2011. DOE Response to the Radiological Release from the Fukushima Dai-Ichi Nuclear Power Plant. *NEI RETS/REMP Workshop*. http://hps.ne.uiuc.edu/rets-remp/PastWorkshops/2011/presentations/6C-DOE Response to the Radiological Release from the Fukushima Daiichi Nuclear Power Plant.pdf

Han, J., and Y. Chen. 2014. "Multiple UAV Formations for Cooperative Source Seeking and Contour Mapping of a Radiative Signal Field." *Journal of Intelligent & Robotic Systems: Theory and Applications* 74: 323–332. doi:10.1007/s10846-013-9897-4.

Han, J., Y. Xu, L. Di, and Y. Chen. 2013. "Low-cost Multi-UAV Technologies for Contour Mapping of Nuclear Radiation Field." *Journal of Intelligent & Robotic Systems* 70 (1–4): 401–410. doi:10.1007/s10846-012-9722-5.

He, K., H. Huo, and Q. Zhang. 2002. "Urban Air Pollution in CHINA: Current Status, Characteristics, and Progress." *Annual Review of Energy and the Environment* 27 (1): 397–431. doi:10.1146/annurev.energy.27.122001.083421.

Howse, J. W., L. O. Ticknor, and K. R. Muske. 2001. "Least Squares Estimation Techniques for Position Tracking of Radioactive Sources." *Automatica* 37 (11): 1727–1737. doi:10.1016/S0005-1098(01)00134-0.

Hubbell, J. H. 1969. Photon Cross Sections, Attenuation Coefficients and Energy Absorption Coefficients from 10 keV to 100 GeV. *National Standard Reference Data Series (NSRDS)*. http://www.nist.gov/srd/nsrds.cfm

IAEA. 2003. Occupational Radiation Protection: Protecting Workers against Exposure to Ionizing Radiation. Accessed November 23 2015. http://www-pub.iaea.org/mtcd/publications/pdf/pub1145_web.pdf

Jiang, J., K. Shimazoe, Y. Nakamura, H. Takahashi, Y. Shikaze, Y. Nishizawa, … A. Yoshikawa. 2015. "A Prototype of Aerial Radiation Monitoring System Using an Unmanned Helicopter Mounting A GAGG Scintillator Compton Camera." *Journal of Nuclear Science and Technology*. doi:10.1080/00223131.2015.1089796.

Jones, H. E., and J. R. Cunningham. 1983. *Physics of Radiology*. 4th ed. Springfield, IL: Thomas.

Karp, S., and L. Stotts. 2012. *Fundamentals of Electro-optic Systems Design: Communications, Lidar, and Imaging*. Cambridge University Press. http://www.cambridge.org/catalogue/catalogue.asp?isbn=9781107021396&ss=fro

Katata, G., M. Ota, H. Terada, M. Chino, and H. Nagai. 2012. "Atmospheric Discharge and Dispersion of Radionuclides during the Fukushima Dai-Ichi Nuclear Power Plant Accident. Part I: Source Term Estimation and Local-Scale Atmospheric Dispersion in Early Phase of the Accident." *Journal of Environmental Radioactivity* 109: 103–113. doi:10.1016/j.jenvrad.2012.02.006.

Kinoshita, N., K. Sueki, K. Sasa, J. Kitagawa, S. Ikarashi, T. Nishimura, Y.-S. Wong, et al. 2011. "Assessment of Individual Radionuclide Distributions from the Fukushima Nuclear Accident Covering Central-East Japan." *Proceedings of the National Academy of Sciences of the United States of America* 108 (49): 19526–19529. doi:10.1073/pnas.1111724108.

Knoll, G. F. 2010. *Radiation Detection and Measurement*. John Wiley & Sons. https://books.google.com/books?hl=en&id=4vTJ7UDel5IC&pgis=1

Kromek Group PLC. 2015. *SIGMA Spec Sheet; Revision 6*. http://www.kromek.com/index.php/products/applications/radiation-detection/gr1-gamma-ray-spectrometer

Kurokawa, K., K. Ishibashi, and K. Oshima. 2012. The Official Report of the Fukushima Nuclear Accident Independent Investigation Commission. *The National Diet of Japan*. https://scholar.

google.com/scholar?q=The+Official+Report+of+the+Fukushima+Nuclear+Accident+Independent+Investigation+Commission#0

Kurvinen, K., P. Smolander, R. Pöllänen, S. Kuukankorpi, M. Kettunen, and J. Lyytinen. 2005. "Design of a Radiation Surveillance Unit for an Unmanned Aerial Vehicle." *Journal of Environmental Radioactivity* 81 (1): 1–10. doi:10.1016/j.jenvrad.2004.10.009.

Leclair, P. 2010. *Gamma Ray Attenuation*. University of Alabama. http://faculty.mint.ua.edu/~pleclair/PH255/templates/formal/formal.pdf

Lozano, R. L., M. A. Hernández-Ceballos, J. A. Adame, M. Casas-Ruíz, M. Sorribas, E. G. San Miguel, and J. P. Bolívar. 2011. "Radioactive Impact of Fukushima Accident on the Iberian Peninsula: Evolution and Plume Previous Pathway." *Environment International* 37 (7): 1259–1264. doi:10.1016/j.envint.2011.06.001.

Luke, P., M. Amman, J. Lee, B. A. Ludewigt, and H. Yaver. 2001. "A Cdznte Coplanar-Grid Detector Array for Environmental Remediation." *Nuclear Instruments and Methods in Physics Research Section A: Accelerators, Spectrometers, Detectors and Associated Equipment* 458: 319–324. doi:10.1016/S0168-9002(00)00876-7.

Luke, P. N. 1995. "Unipolar Charge Sensing with Coplanar Electrodes-Application to Semiconductor Detectors." *IEEE Transactions on Nuclear Science* 42 (4): 207–213. doi:10.1109/23.467848.

MacFarlane, J. W., O. D. Payton, A. C. Keatley, G. P. T. Scott, H. Pullin, R. A. Crane, M. Smilion, I. Popescu, V. Curlea, and T. B. Scott. 2014. "Lightweight Aerial Vehicles for Monitoring, Assessment and Mapping of Radiation Anomalies." *Journal of Environmental Radioactivity* 136: 127–130. doi:10.1016/j.jenvrad.2014.05.008.

Martin, P. G., O. D. Payton, J. S. Fardoulis, D. A. Richards, and T. B. Scott. 2015. "The Use of Unmanned Aerial Systems for the Mapping of Legacy Uranium Mines." *Journal of Environmental Radioactivity* 143: 135–140. doi:10.1016/j.jenvrad.2015.02.004.

Martin, P. G., O. D. Payton, J. S. Fardoulis, D. A. Richards, Y. Yamashiki, and T. B. Scott. 2016. "Low Altitude Unmanned Aerial Vehicle for Characterising Remediation Effectiveness Following the FDNPP Accident." *Journal of Environmental Radioactivity* 151: 58–63. doi:10.1016/j.jenvrad.2015.09.007.

Masson, O., A. Baeza, J. Bieringer, K. Brudecki, S. Bucci, M. Cappai, F. P. Carvalho, et al. 2011. "Tracking of Airborne Radionuclides from the Damaged Fukushima Dai-Ichi Nuclear Reactors by European Networks." *Environmental Science & Technology* 45 (18): 7670–7677. doi:10.1021/es2017158.

Mellander, H. 1995. "The Role of Mobile Gamma Spectrometry in the Swedish Emergency Response Programme for Nuclear Accidents - Experience and Future Plans." *IAEA TECDOC-827, November 1993* 8: 187–195. http://www.iaea.org/inis/collection/NCLCollectionStore/_Public/27/025/27025425.pdf#page=187

Morelande, M., B. Ristic, and A. Gunatilaka. 2007. "Detection and Parameter Estimation of Multiple Radioactive Sources." In *2007 10th International Conference on Information Fusion*, 1–7. IEEE. doi:10.1109/ICIF.2007.4408094.

Muske, K. R., and J. W. Howse. 2001. "Comparison of Recursive Estimation Techniques for Position Tracking Radioactive Sources." In *Proceedings of the 2001 American Control Conference. (Cat. No.01CH37148)*, 1656–1660. Vol. 2. IEEE. doi:10.1109/ACC.2001.945966.

Omoto, A. 2013. "The Accident at TEPCO's Fukushima-Daiichi Nuclear Power Station: What Went Wrong and What Lessons are Universal?" *Nuclear Instruments and Methods in Physics Research Section A: Accelerators, Spectrometers, Detectors and Associated Equipment* 731: 3–7. doi:10.1016/j.nima.2013.04.017.

Ordnance Survey (GB). 2015. OS Terrain 5 [ASC Geospatial Data], Scale 1:10000. st67sw. EDINA Digimap Ordnance Survey Service. Updated December 16 2015, Downloaded February 26 2016. http://digimap.edina.ac.uk

Pöllänen, R., H. Toivonen, K. Peräjärvi, T. Karhunen, T. Ilander, J. Lehtinen, K. Rintala, T. Katajainen, J. Niemelä, and M. Juusela. 2009. "Radiation Surveillance Using an Unmanned Aerial Vehicle." *Applied Radiation and Isotopes* 67 (2): 340–344. doi:10.1016/j.apradiso.2008.10.008.

Povinec, P. P., K. Hirose, and M. Aoyama. 2013. *Fukushima Accident: Radioactivity Impact on the Environment*. Newnes. https://books.google.com/books?hl=en&id=GW6i6pbzKgwC&pgis=1.

Sanada, Y., and T. Torii. 2015. "Aerial Radiation Monitoring around the Fukushima Dai-Ichi Nuclear Power Plant Using an Unmanned Helicopter." *Journal of Environmental Radioactivity* 139: 294–299. doi:10.1016/j.jenvrad.2014.06.027.

Sanderson, D. C. W., J. D. Allyson, A. N. Tyler, and E. M. Scott. 1995. Environmental Applications of Airborne Gamma Spectrometry. http://www.iaea.org/inis/collection/NCLCollectionStore/_Public/27/025/27025425.pdf

Schwarz, G. F., L. Rybach, C. K. Barlocher, and E. E. Klingele. 1995. "Development and Calibration of an Airborne Radiometric Measuring System." *IAEA TECDOC-827, November 1993* 8: 26–35. http://www.iaea.org/inis/collection/NCLCollectionStore/_Public/27/025/27025425.pdf#page=26

Schwarz, G. F., L. Rybach, and E. E. Klingele. 1995. "Data Processing and Mapping in Airborne Radioactivity Surveys." *IAEA TECDOC-827, November 1993* 8: 61–70. http://www.iaea.org/inis/collection/NCLCollectionStore/_Public/27/025/27025425.pdf#page=61

Sellin, P. J. 2003. "Recent Advances in Compound Semiconductor Radiation Detectors." *Nuclear Instruments and Methods in Physics Research, Section A: Accelerators, Spectrometers, Detectors and Associated Equipment* 513 (1–2): 332–339. doi:10.1016/j.nima.2003.08.058.

Shah, K., J. Glodo, M. Klugerman, W. Moses, S. Derenzo, and M. J. Weber. 2003. "Labr/Sub 3/:Ce Scintillators for Gamma-Ray Spectroscopy." *IEEE Transactions on Nuclear Science* 50 (6): 2410–2413. doi:10.1109/TNS.2003.820614.

Shapiro, L., and G. Stockman. 2001. "Computer Vision." *October, 2004*, Oct.: 608. doi:10.1525/jer.2008.3.1.toc.

Sharp, I., K. Yu, and Y. J. Guo. 2009. "Peak and Leading Edge Detection for Time-of-Arrival Estimation in Band-Limited Positioning Systems." *IET Communications* 3 (10): 1616. doi:10.1049/iet-com.2008.0637.

Simons, M., S. E. Minson, A. Sladen, F. Ortega, J. Jiang, S. E. Owen, L. Meng, et al. 2011. "The 2011 Magnitude 9.0 Tohoku-Oki Earthquake: Mosaicking the Megathrust from Seconds to Centuries." *Science (New York, N.Y.)* 332 (6036): 1421–1425. doi:10.1126/science.1206731.

Stefanik, K. V., J. C. Gassaway, K. Kochersberger, and A. L. Abbott. 2013. "UAV-Based Stereo Vision for Rapid Aerial Terrain Mapping." *GIScience & Remote Sensing*. doi:10.2747/1548-1603.48.1.24.

Thrun, S. 2002. "Probabilistic Robotics." *Communications of the ACM* 45 (3): 52–57. doi:10.1145/504729.504754.

Towler, J., B. Krawiec, and K. Kochersberger. 2012. "Radiation Mapping in Post-Disaster Environments Using an Autonomous Helicopter." *Remote Sensing* 4 (12): 1995–2015. doi:10.3390/rs4071995.

Uher, J., C. Frojdh, J. Jakubek, S. Pospisil, G. Thungstrom, and Z. Vykydal. 2007. "Directional Radiation Detector." In *2007 IEEE Nuclear Science Symposium Conference Record*, 1162–1165. Vol. 2. IEEE. doi:10.1109/NSSMIC.2007.4437213.

Wilson, M. D., R. Cernik, H. Chen, C. Hansson, K. Iniewski, L. L. Jones, P. Seller, and M. C. Veale. 2011. "Small Pixel CZT Detector for Hard X-Ray Spectroscopy." *Nuclear Instruments and Methods in Physics Research Section A: Accelerators, Spectrometers, Detectors and Associated Equipment* 652 (1): 158–161. doi:10.1016/j.nima.2011.01.144.

World Health Organization. 1999. Guidelines for Iodine Prophylaxis following Nuclear Accidents: Update 1999. http://apps.who.int/iris/handle/10665/66143

Yasunari, T. J., A. Stohl, R. S. Hayano, J. F. Burkhart, S. Eckhardt, and T. Yasunari. 2011. "Cesium-137 Deposition and Contamination of Japanese Soils Due to the Fukushima Nuclear Accident." *Proceedings of the National Academy of Sciences of the United States of America* 108 (49): 19530–19534. doi:10.1073/pnas.1112058108.

Yoshida, N., and J. Kanda. 2012. "Geochemistry. Tracking the Fukushima Radionuclides." *Science (New York, N.Y.)* 336 (6085): 1115–1116. doi:10.1126/science.1219493.

Zhang, Q., C. Zhang, Y. Lu, K. Yang, and Q. Ren. 2013. "Progress in the Development of Cdznte Unipolar Detectors for Different Anode Geometries and Data Corrections." *Sensors (Basel, Switzerland)* 13 (2): 2447–2474. doi:10.3390/s130202447.